PERGAMON

Journal of Atmospheric and Solar-Terrestrial Physics 64 (2002) 1911–1931

Journal of ATMOSPHERIC AND SOLAR-TERRESTRIAL PHYSICS

www.elsevier.com/locate/jastp

Modelling F2-layer seasonal trends and day-to-day variability driven by coupling with the lower atmosphere

M. Mendillo[a], H. Rishbeth[a,b,*], R.G. Roble[c], J. Wroten[a]

[a] *Center for Space Physics, Boston University, Boston, MA02215, USA*
[b] *Department of Physics and Astronomy, University of Southampton, Southampton SO17 1BJ, UK*
[c] *High Altitude Observatory, National Center for Atmospheric Research, Box 3000, Boulder CO80301, USA*

Received 10 December 2001; received in revised form 6 May 2002; accepted 14 June 2002

Abstract

This paper presents results from the TIME-GCM-CCM3 thermosphere–ionosphere–lower atmosphere flux-coupled model, and investigates how well the model simulates known F2-layer day/night and seasonal behaviour and patterns of day-to-day variability at seven ionosonde stations. Of the many possible contributors to F2-layer variability, the present work includes only the influence of 'meteorological' disturbances transmitted from lower levels in the atmosphere, solar and geomagnetic conditions being held at constant levels throughout a model year.

In comparison to ionosonde data, TIME-GCM-CCM3 models the peak electron density (*N*mF2) quite well, except for overemphasizing the daytime summer/winter anomaly in both hemispheres and seriously underestimating night *N*mF2 in summer. The peak height *h*mF2 is satisfactorily modelled by day, except that the model does not reproduce its observed semiannual variation. Nighttime values of *h*mF2 are much too low, thus causing low model values of night *N*mF2. Comparison of the variations of *N*mF2 and the neutral $[O/N_2]$ ratio supports the idea that both annual and semiannual variations of F2-layer electron density are largely caused by changes of neutral composition, which in turn are driven by the global thermospheric circulation.

Finally, the paper describes and discusses the characteristics of the F2-layer response to the imposed 'meteorological' disturbances. The ionospheric response is evaluated as the standard deviations of five ionospheric parameters for each station within 11-day blocks of data. At any one station, the patterns of variability show some coherence between different parameters, such as peak electron density and the neutral atomic/molecular ratio. Coherence between stations is found only between the closest pairs, some 2500 km apart, which is presumably related to the scale size of the 'meteorological' disturbances. The F2-layer day-to-day variability appears to be related more to variations in winds than to variations of thermospheric composition.

Keywords: Ionosphere; F2-layer; Ionospheric variability; Lower atmosphere-upper atmosphere coupling

1. Introduction

There now exists a reasonably good understanding of photochemical, thermodynamic and electrodynamic processes in the ionospheric F-layer under quiet conditions. This is largely due to the development of theoretical models of the thermosphere–ionosphere system that successfully match many observed features of the peak electron density *N*mF2 and other F-layer properties. Anderson et al. (1998) compared the daily variations of *N*mF2 and *h*mF2 given by five global models at solar minimum and maximum at one midlatitude site, Millstone Hill, for geomagnetically quiet conditions. The 'coupled models' that

* Corresponding author. Department of Physics & Astronomy, University of Southampton, Southampton SO17 1BJ, UK. Tel.: +44-0-2380-592048; fax: +44-0-2380-593910.
E-mail address: hr@phys.soton.ac.uk (H. Rishbeth).

1364-6826/02/$ - see front matter
PII: S1364-6826(02)00193-1

self-consistently compute the parameters of the neutral and ionized gases, namely the 'Thermosphere–ionosphere–mesosphere–electrodynamics general circulation model' (TIME-GCM), essentially as used in this paper, and the 'Coupled thermosphere–ionosphere–plasmasphere' model (CTIP, Millward et al., 1996a), agree quite well in their mean values of NmF2 and the peak height hmF2 with the three 'non-coupled' models, in which the neutral temperature and composition are prescribed by the MSIS model of Hedin (1987) and the winds by the HWM model (Hedin et al., 1991). More severe challenges are presented by the day-to-day variability of the F2-layer, and also by ionospheric storms which the present paper does not consider.

This paper uses a 'flux-coupled' version of TIME-GCM for two main purposes: first, to explain features of the large-scale structure of the quiet F2-layer, as observed at seven representative midlatitude sites; second, to study at these sites the day-to-day effects in the F2-layer of disturbances generated by the 'Community Climate Model' (CCM3, the lower atmosphere part of the composite flux-coupled model) and propagated to the ionosphere. We call these 'meteorological' disturbances.

Besides the meteorological (lower atmosphere) forcings considered in this paper, the causes of ionospheric variability include solar activity, the seasonal and diurnal variations of solar zenith angle, the eccentricity of the Earth's orbit, geomagnetic activity, and plasmaspheric and magnetospheric influences (some of which are also linked to geomagnetic activity). Features of the observed variability of the peak F2-layer electron density NmF2, and how this variability differs between day and night and with season and solar cycle, have a long history of study, with the most recent work by Forbes et al. (2000), Fuller-Rowell et al. (2000) and Rishbeth and Mendillo (2001).

Previous results have shown that the lower atmosphere introduces variability into the upper atmosphere by upward propagation, dissipation and reflection and interference of large scale waves and the filtering of gravity waves by dynamical structures in the lower atmosphere. In general, it is the large scale waves that propagate highest into the thermosphere. Electron density in the F-region can be affected by direct dynamic forcing, changes in temperature and composition, and E-region dynamo electric fields that produce drifts in the F-region, though it is difficult to separate these effects in the simulations. A description of some of the results calculated by the coupled models is given by Roble (2000). Observations of the variability of thermospheric neutral winds and airglow, made by instruments aboard the UARS satellite, have been reported by Wiens et al. (1999), Fejer et al. (2000) and Thuillier et al. (2002), and from ground-based radio and optical measurements by Martinis et al. (2001) and Fesen et al. (2002). These observations were mostly made at fairly low latitudes, while our present study is concerned with midlatitudes.

The flux-coupling of two dissimilar models at an interface in the free atmosphere is an exploratory exercise to obtain some idea on how a self-consistent model of the entire atmosphere would behave. It is basically a feasibility study to investigate how processes in the lower atmosphere affect the upper atmosphere. From previous studies using TIME-GCM only, it is clear that solar and auroral variability alone cannot represent the day-to-day variability observed by ground-based and satellite instruments, especially in the upper mesosphere and lower thermosphere. Another motivation for the development of a GCM of the entire atmosphere is to examine how deeply solar-terrestrial effects penetrate into the Earth's atmosphere.

The coupled model runs freely, generating its own internal variability, and thus does not simulate any specific day that can be compared with measurements for that day. However, the mean structure for a given month can be compared with the corresponding averaged data. The model should give the mean tidal structure, should generate stratospheric warmings, and should have a semiannual variation, etc., so in this sense it can be 'calibrated'.

As described in Section 2, we ran the TIME-GCM-CCM3 flux-coupled model for an idealized 365-day year in which solar activity is kept constant at a moderate level, only the variations due to seasonal changes of solar declination and Sun–Earth distance being included, and geomagnetic activity is very low. In Section 3 we discuss the seasonal variations of thermospheric and F2-layer parameters and compare the model outputs with monthly averaged ionosonde data from seven representative midlatitude stations, considering how well the model reproduces known seasonal and semiannual variations. Section 4 uses the height-independent 'P-parameter', as defined by Rishbeth and Müller-Wodarg (1999), to show that the seasonal changes of F2-layer electron density are mostly due to changes of neutral composition.

With an understanding of how the model behaves with seasonal changes of solar declination as the sole driver of variability, we consider in Sections 5 and 6 the effects that appear with the additional driver of lower atmosphere 'weather' as portrayed by CCM3. In Section 5 we consider the results from the seven midlatitude stations, and find that the disturbances originating in the CCM3 simulation cause variations of 10–30% in F2-layer electron density. In Section 6 we consider in more detail some particular episodes, mainly at one station (Port Stanley) where the 'meteorological' disturbances seem particularly severe. We sum up our findings in Section 7.

2. The TIME-GCM-CCM3 flux-coupled model

2.1. Flux-coupling of the thermospheric and lower atmosphere models

To obtain some insight into how the variability of the lower atmosphere affects the upper atmosphere, the TIME-GCM has been flux-coupled to the NCAR community

climate model CCM3. The CCM3, described by Kiehl et al. (1998), is a spectral model with a horizontal T42 spectral resolution (approximately $2.8^\circ \times 2.8^\circ$ transform grid) and has 18 pressure surfaces extending between the ground and the 2.9 mb level (about 40 km height). The model time step is 20 min and includes a diurnal cycle in which radiative fluxes are calculated every hour.

TIME-GCM is a finite difference grid point model with fourth order horizontal differencing on a $5^\circ \times 5^\circ$ latitude/longitude grid. It has 45 pressure surfaces extending from 10 mb (about 30 km height) to above 500 km with a vertical resolution of 2 grid points per scale height and a model time step of 5 min. For the flux-coupled mode the lower boundary has been raised to the 2.9 mb level, the upper boundary pressure of CCM3. It includes a diurnal cycle for all chemical species and physical processes.

To couple the two models a message-passing flux-coupler is used to synchronize the model time steps and provide the interpolation of quantities in both time and space that are passed between the two models, as described by Roble (2000). Thus information at the CCM3 upper boundary is transferred to the lower boundary of TIME-GCM and vice versa. The physical quantities used in the transfer are temperature, zonal and meridional winds, geopotential height and the mass mixing ratios of water vapour and methane. Since the time constants are much longer in CCM3, the combined models are started from a 10 year run of CCM3 in a stand-alone simulation, which gives ample time for settling-down before the coupled TIME-GCM-CCM3 run is started.

Except for certain long-lived chemical species in the TIME-GCM, the temperature and dynamics of the middle and upper atmosphere adjust to any imposed lower boundary forcing in about 20 days of simulation time. Therefore, the coupled models are allowed to adjust for 3 months before histories are recorded for analysis. The primary motivation for this initial investigation is to determine how variability generated in the lower atmosphere propagates into the upper atmosphere and ionosphere. The replacement of the 'rigid lid' upper boundary of CCM3 with the TIME-GCM has some effect on the upper stratosphere layers within CCM3, but generally the effect does not propagate deeply into the stratosphere. We ran the flux-coupled model for three complete and identical years with constant solar activity ($F_{10.7} = 140$) and quiet geomagnetic conditions (see next section). This paper uses the outputs for the third and final year.

2.2. The present version of TIME-GCM

The NCAR thermosphere–ionosphere–mesosphere–electrodynamics general circulation model (TIME-GCM) (Roble, 1996) is the latest in a series of three-dimensional time-dependent models that have been developed over the past two decades to simulate the circulation, temperature, and compositional structure of the upper atmosphere and ionosphere. It combines all the previous features of the TGCM as described by Dickinson et al. (1981, 1984), TIGCM (Roble et al., 1987, 1988) and TIE-GCM (Richmond et al., 1992). The model has been extended downward to 30 km altitude, including aeronomic processes appropriate for the mesosphere and upper stratosphere, as described by Roble and Ridley (1994), and Roble (1995). The differences between the model described in previous papers and that used for the present work include the following:

1. Solar ionization rates are calculated using the EUVAC solar flux model and absorption cross-sections from Richards et al. (1994). Solar photodissociation rates for the mesosphere and upper stratosphere are determined using the parameterizations given in Brasseur and Solomon (1986) and Zhao and Turco (1997).
2. The chemical reaction rates for the aeronomic scheme described by Roble (1995) have been updated to be consistent with the JPL-97 compilation (DeMore et al., 1997).
3. The background diffusion used by Roble and Ridley (1994) has been reduced by two orders of magnitude, consistent with the findings of Akmaev et al. (1996) in their simulation of the diurnal tide. The background diffusion and Rayleigh friction are now very small throughout the model.
4. The CO_2 infrared cooling parameterization has been updated to include the model of Fomichev et al. (1998) to account for a variable CO_2 mixing ratio, important for non-LTE (local thermal equilibrium) processes in the upper mesosphere and lower thermosphere. All calculations assume an O–CO_2 vibrational relaxation rate of 3×10^{-12} cm^{-3} s^{-1}, which works reasonably well for terrestrial planetary thermospheres (Bougher et al., 1999).

2.3. Dynamical coupling between the lower atmosphere and thermosphere

The key component of the new model is dynamical coupling from below. Since the TIME-GCM grid is 5° in latitude and longitude, larger scale ($\sim$1000's km) planetary waves propagate directly from CCM3 to TIME-GCM. A gravity wave parameterization for waves smaller in scale than the TIME-GCM grid ($\sim$10's–100's km) is necessary to obtain the observed mesospheric structure. The scheme of Lindzen (1981) is used in the present simulations and the prescribed forcing at the lower boundary varies with latitude as described by Roble (2000). This gravity wave flux is constant throughout the year at the 30 mb boundary level; but its transmission to higher levels is affected by the planetary wave structure of the variability introduced from CCM3, and is strongest in the northern hemisphere during winter. See Roble (2000) for further details.

There are no tides imposed artificially at the lower boundary of the TIME-GCM. The diurnal tidal forcing comes from tropospheric sources in CCM3 as transmitted through the boundary into the TIME-GCM. The semidiurnal tidal

forcing also comes from the tropospheric forcings, but there is an additional self-consistent component from middle and upper atmospheric heating by ozone and molecular oxygen, as discussed by Hagan et al. (2001).

Within the model year, localized disturbances arise internally within CCM3. No disturbances have been forcibly imposed on CCM3, so the ionospheric phenomena may be assumed to represent behaviour that can arise naturally. In general, synoptic-scale disturbances such as tropospheric weather fronts, or waves generated by low pressure systems do not propagate into the upper atmosphere (Andrews et al., 1987). Larger scale planetary waves of wavenumbers 1 or 2 can propagate into the mesosphere during winter when the mean zonal winds are eastward, but they are absorbed during summer and confined to the lower atmosphere; the ionospheric variability described here is most likely due to propagation of planetary scale waves in the winter hemisphere, and in particular to the filtering by winds of the vertically propagating gravity waves that deposit their momentum and heat in the thermosphere (Smith, 1996).

Once these waves are transmitted dynamically upward through the mesosphere to the base of the thermosphere, they appear as episodic disturbances that are dissipated by molecular diffusion, thermal conductivity and ion drag in the lower thermosphere. The effects they produce in that region can be transmitted to the F-region by molecular diffusion, dynamo action or large scale circulation changes. Planetary scale waves with large vertical wavelengths, such as the semidiurnal tide, can also propagate to high altitudes. These disturbances are the subject of Sections 5 and 6 of this paper.

2.4. Ionospheric inputs and outputs

TIME-GCM calculates the heating, photoionization, dynamics and compositional structure of the middle and upper atmosphere and ionosphere for a given solar irradiance spectrum, which in the present version is computed for solar radio flux $F_{10.7} = 140$, held constant throughout the entire model run. The geomagnetic activity is held constant at a very quiet level ($A\mathrm{p} = 4$), and the model includes a cross-polar cap potential of 45 kV, auroral hemispheric power input of 15 GW, and the corresponding level of auroral precipitation as described by Roble and Ridley (1987).

Since the present model does not include the appropriate physics to represent the exchange of plasma and energy between the magnetosphere and ionosphere, it is necessary to parameterize these fluxes. It is assumed that there is an upward flux of plasma (O^+, e^-) into the plasmasphere during the daytime (solar zenith angle $< 100^\circ$) of $2.8 \times 10^8\ \mathrm{cm^{-2}\ s^{-1}}$ and a downward flow $-2.8 \times 10^8\ \mathrm{cm^{-2}\ s^{-1}}$ at night (solar zenith angle $> 100^\circ$), both multiplied by an empirical function of magnetic latitude up to 60°. A constant polar wind outflow of $1 \times 10^8\ \mathrm{cm^{-2}\ s^{-1}}$ is maintained at all higher latitudes. In the summer hemisphere, the total upward flux is larger because of the long daylight hours. The flux is approximated to obtain reasonable topside densities in accordance with the International Reference Ionosphere (IRI, Bilitza et al., 1993). This assumption leads to higher winter densities and lower summer densities, especially at night where the model/data disagreement is greatest. There is a clear need for a more physically based upper boundary condition for the ionospheric plasma flow and this work is in progress.

The present study uses TIME-GCM-CCM3 outputs for seven ionosonde stations at midlatitudes (Table 1), chosen to represent different geographic and geomagnetic latitudes and longitudes, and for their long-term sequences of reliable observations. The output parameters used here are the peak electron density NmF2, the atomic oxygen/molecular nitrogen concentration ratio of the neutral air [O/N_2], the height hmF2 of the F2 peak, the neutral gas temperature T_n, and the meridional (south-to-north) wind speed U_m. The parameters are interpolated between the pressure-levels to give the values at the F2 peak for days 1–365 of the model year. The discussion mostly concentrates on two local times, 02:00 LT and 12:00 LT.

3. Seasonal quiet-day variations of TIME-GCM model parameters

3.1. Variation of peak electron density NmF2 throughout the year at seven stations

For comparison with the TIME-GCM model outputs for solar decimetric flux $F_{10.7} = 140$ units, the ionosonde data are taken from the years 1960, 1967, 1970, 1978, 1983, and 1988, with annual mean fluxes in the range 120–160 (average 144). Table 1 gives details of the seven stations. Fig. 1 shows the month-by-month results for six stations, omitting Moscow which behaves quite similarly to Slough. The shading shows the ± standard deviation from the monthly mean of ionosonde values recorded on all the individual days in all the years; the distinct daily curves are the model outputs for days 1–365. Although the day numbers cannot be shown in Fig. 1, the daily curves near equinox, where solar conditions are changing most rapidly, show a regular progression from winter to summer or vice versa, which is only slightly interrupted by the 'meteorological' disturbances. Table 2 shows monthly noon model/ionosonde ratios of NmF2 at each station. To indicate how well the model represents the ionosonde data, we show the 'mean deviation' for each station, which is the average of the 12 monthly 'deviations' $|(\mathrm{model/ionosonde}) - 1|$ without regard to sign. On this criterion, Port Stanley and Brisbane are the best modelled stations.

As the model outputs assume magnetically quiet conditions ($A\mathrm{p} = 4$), they pertain to the most quiet (QQ) days. The ionosonde data are monthly means and therefore incorporate an average level of magnetic activity, about 15 units of Ap according to Rishbeth and Mendillo (2001). The geomagnetic influence in the model outputs is thus smaller

Table 1
Station geographic and magnetic coordinates

Station	Geog. lat.	Geog. long.	Dip. lat.	Lat. diff.	UT at noon
Moscow	+56	+37	+55	+1	09
Slough	+52	−1	+50	+2	12
Wallops Is	+39	−77	+52	−13	17
Wakkanai	+45	+142	+39	+6	03
Brisbane	−28	+153	−39	−11	02
Hobart	−43	+147	−58	−15	02
Port Stanley	−52	−58	−30	+22	16

Dip latitude (Dip Lat) is derived from the magnetic dip angle I by the idealized dipole equation (dip latitude) = arc tan (1/2 tan I). 'Lat. Diff' is the numerical difference between the latitudes, viz |Geog.Lat| − |Dip. Lat|.

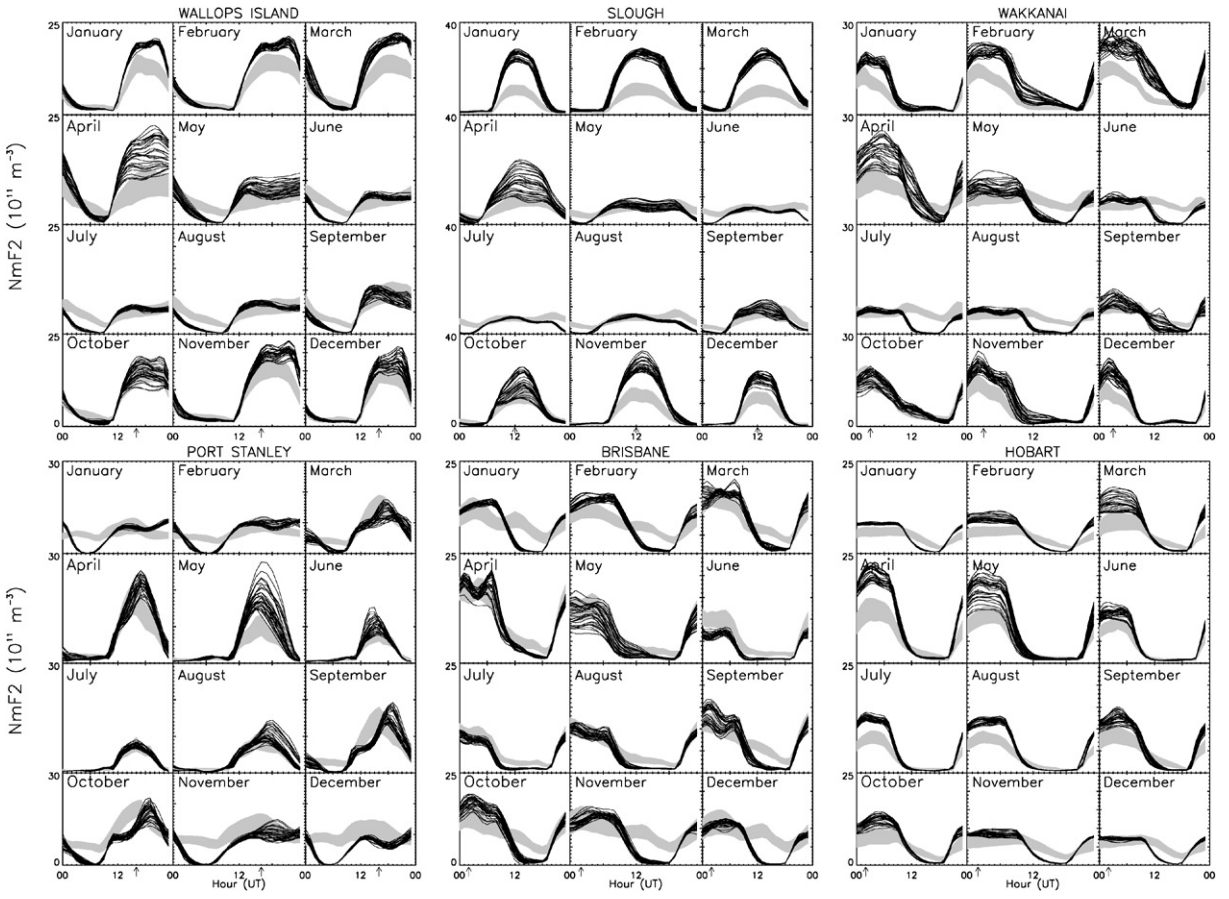

Fig. 1. Month-by-month NmF2 versus Universal Time for model and data for six stations. The shading shows the 1σ range of monthly mean ionosonde values observed during 6 years of average solar activity (mean solar 10.7 cm flux =144 units). The lines are daily values from the TIME-GCM-CCM3 model for a model year (10.7 cm flux =140 units, Ap = 4) with 'meteorological' disturbances transmitted from the lower atmosphere. Arrows show local noon.

than in the ionosonde data, and this would have to be considered in more precise validations of the model. With this caveat, the general conclusions from comparing model and data are as follows. On the whole, TIME-GCM represents the data quite well, but badly overestimates the winter values at Slough (also Moscow), somewhat less so at lower midlatitudes (Wallops Island and Wakkanai). Summer noon is better modelled at all stations, though in some cases—particularly in the south—the shape of the daily variation is wrong, the local time of daytime maximum being some

Table 2
Midday NmF2: TIME-GCM-CCM3/ionosonde ratios

Station	Jan.	Feb.	Mar.	Apr.	May	June	July	Aug.	Sept.	Oct.	Nov.	Dec.	Mean |Dev|
Moscow	2.7	3.0	2.5	2.0	0.9	0.8	0.9	1.0	1.1	1.7	2.3	1.8	0.8
Slough	2.3	2.4	2.5	2.1	1.0	1.0	1.1	1.2	1.0	1.5	2.2	1.6	0.7
Wakkanai	1.7[a]	1.5[a]	1.5[a]	1.7	1.2	1.4	1.2	1.1	1.2	1.0	1.4	1.6	0.4
Wallops Is	1.5	1.3	1.5	1.9	1.0	1.3[b]	1.2[b]	1.1	1.0[b]	1.0	1.3	1.3	0.3
Brisbane	1.2[a]	1.4[a]	1.2[a]	1.1	0.8	0.7	0.9	1.0	1.2	1.3	1.0[a]	1.0[a]	0.2
Hobart	1.3	1.7	1.7	1.7	1.3	1.7	1.6	1.4	1.4	1.6	1.2	1.1	0.5
Port Stanley	1.0	1.0	0.9	1.2	1.7	1.3	1.0	1.1	1.1[a]	0.9[a]	0.9[a]	0.8[a]	0.2

Model outputs are for magnetically quiet conditions; ionosonde data are monthly means (see text). In some cases the noon ionosonde NmF2 is compared with the maximum given by the model, which can occur 2–3 h earlier or later.

[a]Indicates discrepancies in LT of maximum NmF2 if model is 2–3 h later than ionosonde data.

[b]Indicates discrepancies in LT of maximum NmF2 if model is 2–3 h earlier than data. The 'mean deviation' for each station is the mean of the 12 monthly departures from the ideal value of 1.0 (without regard to sign) of the tabulated model/ionosonde ratios.

hours different in model and data. In the north, the model shows a strong transition in April from the (too high) winter values to summer values. So TIME-GCM exaggerates the equinox transition and thus produces a variability that is systematic but too dramatic. October similarly shows too large a transition from summer to winter, thereby enhancing the appearance of variability. Thus for sites with an annual pattern (i.e., Slough, Moscow, Wallops Island), the model appears seasonally 'over-tuned'. The model does well for sites with a semiannual pattern, such as Port Stanley, though the April/May (fall) peak in the south is more pronounced in the model outputs than in the ionosonde data.

At night the situation is reversed: the nighttime patterns have a strong annual pattern, contrary to observations, and NmF2 is modelled quite well in winter. However, the summer model values are far too low in both hemispheres, very likely because the model gives quite low heights of the night F2-peak, resulting in rapid loss of ionization after sunset. Night NmF2 is well modelled at fall equinox in both hemispheres, but is far too low at spring equinox, as in summer. The model's successful portrayal of winter nights (which has been a long-standing ionospheric problem) is related to the downward flux from the protonosphere described in Section 2.2.

3.2. Variations of NmF2 and the neutral $[O/N_2]$ ratio

The upper three panels of each station set in Fig. 2 (for noon, 12:00 LT) and Fig. 3 (for night, 02:00 LT) show the variation throughout the model year of NmF2 and $[O/N_2]$ and their ratio NmF2/$[O/N_2]$ (again omitting Moscow, its characteristics being very similar to Slough's). In these figures and others later in the paper, the numerical scales are chosen to make good use of the available space, so the upper and lower bounds may vary from one station to another.

Notice the strong resemblance between the seasonal variations of NmF2 and $[O/N_2]$ in Fig. 2 (and for that matter, between their day-to-day fluctuations, as we discuss in Sections 5 and 6); indeed, at most stations the ratio (NmF2/$[O/N_2]$) is fairly constant throughout the year. Going from north to south, there is a progressive transition from the February/November peaks of NmF2 (and $[O/N_2]$ too) at northern latitudes to the May/July peaks in southern latitudes, much as described in ionosonde data by Burkard (1951) and King and Smith (1968) and demonstrated by the CTIP modelling of Zou et al. (2000). At night (Fig. 3) the relation between NmF2 and $[O/N_2]$ is not nearly so close, which is to be expected because of the much weaker photochemical control, and NmF2 is largely determined by transport processes, so the ratio NmF2/$[O/N_2]$ is not a useful guide to the physics at night.

We have assumed that molecular nitrogen makes the major contribution to the electron loss process for F2-layer ionization. Although molecular oxygen does contribute to the loss process, that should not significantly affect our conclusions.

3.3. Winds, temperature and the peak height hmF2

The lower three panels of each station set in Figs. 2 and 3 give the model values of hmF2, T_n and U_m, also computed at the F2-peak. In TIME-GCM the height step is half a scale height, corresponding to about 25 km at the daytime F2-peak, and the fitting procedure used to derive hmF2 should be accurate to about one-third of a height step, say 8 km. We now consider the relationship between hmF2, meridional wind and temperature.

The meridional wind U_m is generally poleward at noon (northward (+) in the northern hemisphere, southward (−) in the southern), thus tending to depress hmF2 and hence NmF2, while at night it is generally equatorward (southward (−) in the northern hemisphere, northward (+) in the southern), thus tending to raise hmF2 and hence NmF2. Strictly speaking, the vertical ion drift and the resulting effect on hmF2 is determined by the wind in the *magnetic* meridian, not the *geographic* meridian, so the zonal wind contributes to the vertical drift at places with a large east or west magnetic declination. We neglect this complication

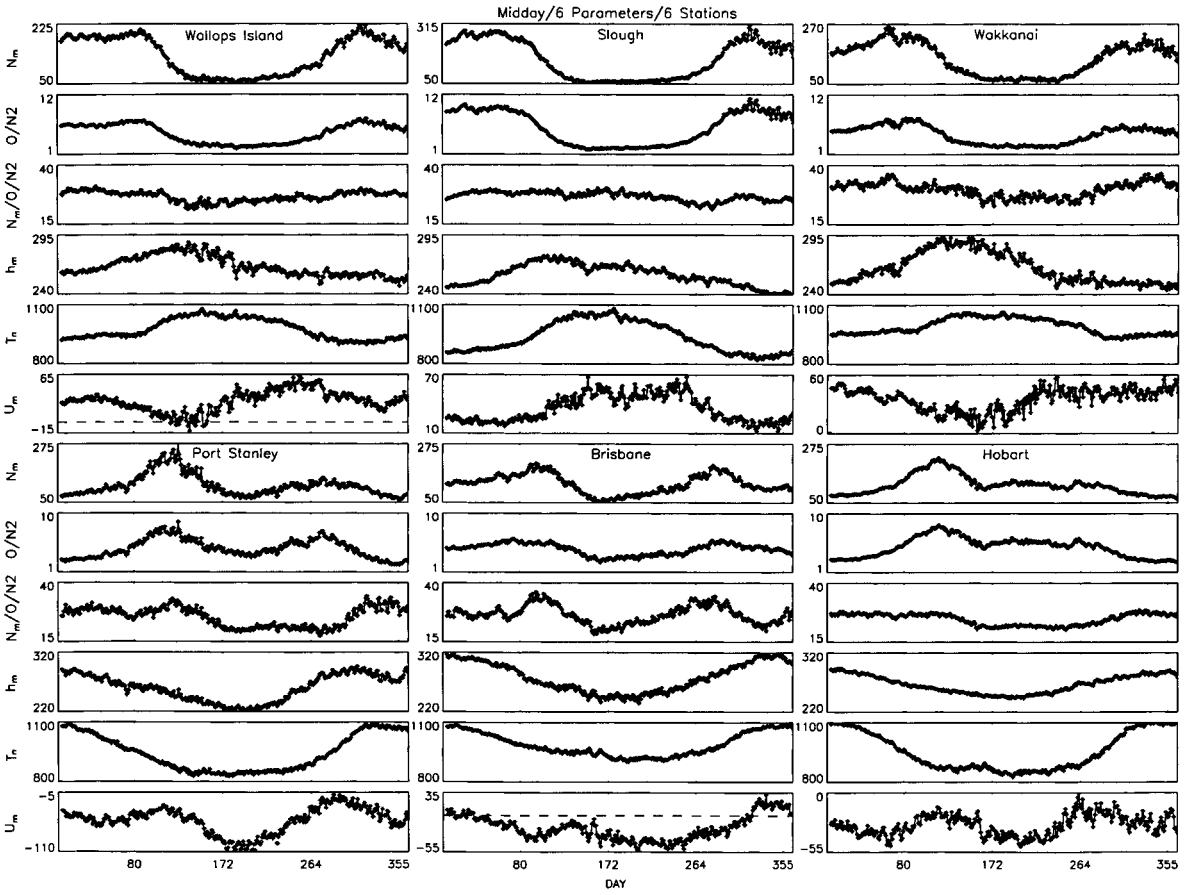

Fig. 2. Variation at midday (12:00 LT) throughout the model year of six parameters at the F2 peak: NmF2 (10^{10} m^{-3}), [O/N_2], the ratio $R = N$mF2/ [O/N_2], hmF2(km), T_n(K) and U_m (m s^{-1} positive northwards), for six stations from TIME-GCM-CCM3 (solar 10.7 cm flux =140 units, $Ap = 4$) with 'meteorological' disturbances transmitted from the lower atmosphere. The zero level of U_m is shown by a dashed line.

because our stations have quite small magnetic declinations (the greatest numerically being that of Hobart, 13°E). The vertical ion drift is related to the horizontal wind speed by the factor cos I sin I, which is greatest (0.5) at magnetic dip angle $I = 45°$ (dip latitude 27°) in either hemisphere. Wind effects are most marked at Port Stanley for two reasons, first because the dip latitude (−30°) is close to the optimum, and second because of the strong winds in this sector, of order 100 m s^{-1} at noon in winter and 200 m s^{-1} at night in summer.

At noon (Fig. 2), the temperature T_n is basically solar controlled, and is fairly symmetrical about the solstices. The height hmF2 is influenced by thermal expansion and contraction of the neutral thermosphere, the F2 peak being approximately barometric (Rishbeth and Edwards, 1989). Consequently, the annual patterns of hmF2 and T_n are quite similar. But although the temperature peaks near midsummer, hmF2 varies in a more complicated way, because the effects of the meridional wind are different in the two hemispheres. In the north, hmF2 peaks in late spring, around days 120–140, which at Wallops Island and Wakkanai is partly because the poleward wind abates in spring. At southern stations, hmF2 peaks at midsummer or slightly earlier (days 300–350), and there is little correlation between changes of hmF2 (or, for that matter, of NmF2) and changes in U_m.

At night (Fig. 3), the hmF2 behaviour is controlled jointly by thermal effects and equatorward winds. Some of the smaller-scale variability seems to result primarily from winds (e.g., midyear at Wallops Island, and days near 270 at Brisbane and Hobart). We return to this in Section 6.

It is not obvious how the hemispheric differences of winds and F2-peak height could arise within the thermosphere, in which the only real north/south difference is in the geomagnetic field configuration. The explanation may lie in coupling to the dynamics of the middle and lower atmosphere, which may well be different in the two hemispheres, but we do not pursue this topic here.

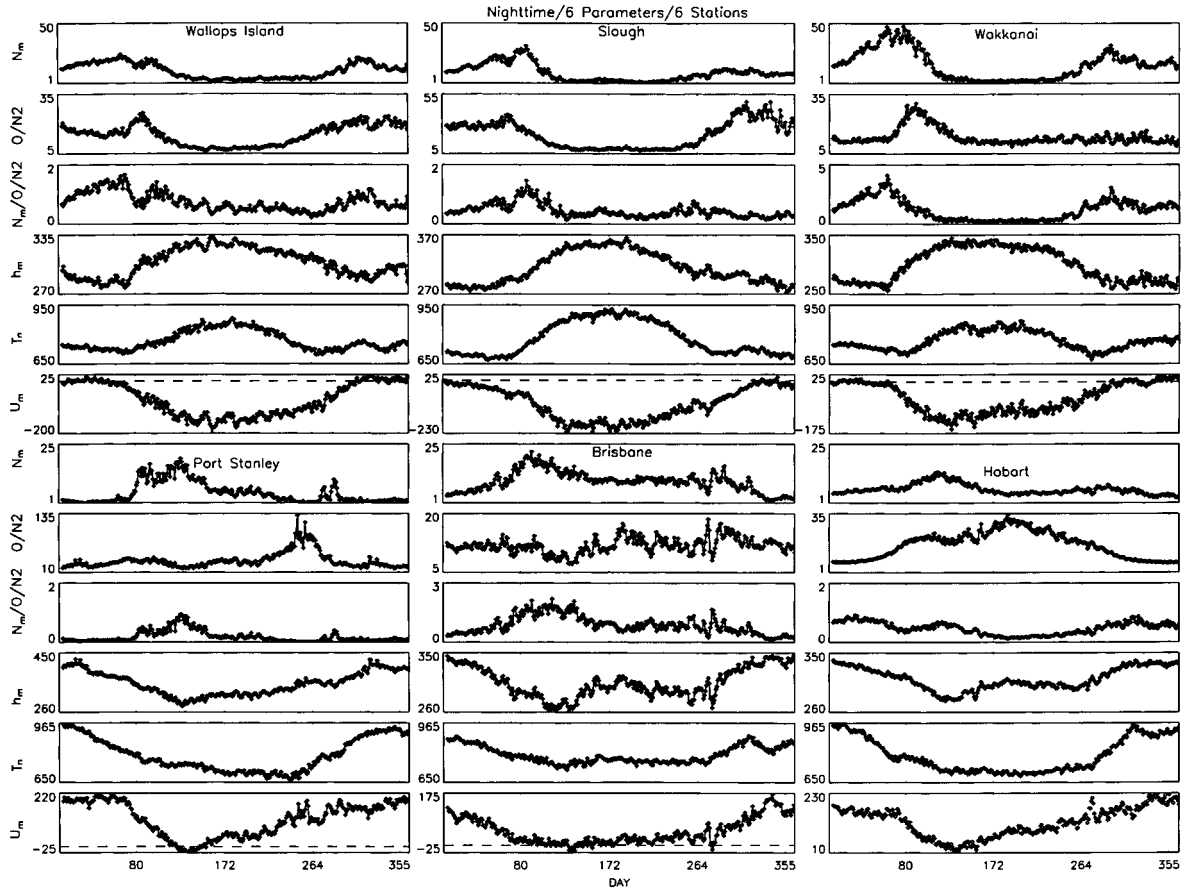

Fig. 3. Variation at night (02:00 LT) throughout the model year of six parameters at the F2 peak: NmF2 (10^{10} m^{-3}), [O/N_2], the ratio, $R = N$mF2/[O/N_2], hmF2 (km), T_n(K) and U_m (m s^{-1} positive northwards), for six stations from TIME-GCM-CCM3 (solar 10.7 cm flux =140 units, $Ap = 4$) with 'meteorological' disturbances transmitted from the lower atmosphere.

3.4. Fourier analysis of NmF2

So far the discussion has concentrated on day-to-night differences rather than month-to-month variations. The latter may conveniently be specified by way of the Fourier components of NmF2 shown in Tables 3 and 4 (12:00 LT) and (02:00 LT), though the Fourier analysis does not necessarily reveal any new physics. We define amplitudes and phases as in the equation

$$N\text{mF2} = N_0 + N_1 \cos((\pi/6)(t - \Phi_{N1})) + N_2 \cos((\pi/3)(t - \Phi_{N2})), \quad (1)$$

where N_0, N_1, N_2 are respectively the mean, annual amplitude, semiannual amplitude; t specifies time in months; and the phase Φ represents the time of maximum in months from December solstice. Analogous equations are applied to hmF2 and the neutral [O/N_2] ratio in Sections 3.5 and 3.6. For the purposes of Fourier analysis, the monthly values are smoothed over about 10 days around midmonth to remove the short-term 'meteorological' fluctuations.

In our discussion we concentrate on the relative amplitudes of the components, and do not compare in detail the model and ionosonde values of the mean values N_0 (which may be regarded as a matter of 'calibration'). The semiannual component consistently peaks near or just after equinox (3.0 months). In contrast, the annual component peaks in winter at northern stations, which all show a 'seasonal anomaly' (winter noon NmF2 > summer noon NmF2), for both model and data. Similar behaviour is seen at Hobart in the south, but not at Port Stanley and Brisbane. There are longitude differences, the annual (winter) component being more pronounced in sectors nearer to the magnetic poles (Moscow, Slough, Wallops Island, Hobart) than in those far from the magnetic poles (Wakkanai, Port Stanley). The semiannual component is more prominent in the sectors far from the magnetic poles (Rishbeth, 1998).

By day (Table 3), at all stations where the annual component is dominant, TIME-GCM overestimates N_0 and N_1 but

Table 3
Model-data comparisons for midday NmF2, 12 LT: amplitudes and phases from TIME-GCM model, $F_{10.7} = 140$

Station	Time-GCM-CCM3						Ionosonde data					
	Amplitude (10^{10} m^{-3})				Phase (month)		Amplitude (10^{10} m^{-3})				Phase (month)	
	N_0	N_1	N_2	N_2/N_1	Φ_{N_1}	Φ_{N_2}	N_0	N_1	N_2	N_2/N_1	Φ_{N_1}	Φ_{N_2}
Moscow	175	139	13	0.1	1.0	3*	97	35	12	0.3	0.0	4*
Slough	161	114	12	0.1	0.9	3*	94	38	12	0.3	0.1	4*
Wakkanai	146	74	29	0.4	1.3	3.5	101	38	30	0.8	0.8	3.4
Wallops Is	135	72	16	0.2	0.9	4*	106	52	12	0.2	0.2	4*
Brisbane	124	24	40	1.7	1.1	3.3	120	17	22	1.3	2.0	3.7
Hobart	120	40	29	0.7	5.2	3.7	80	17	15	0.9	5.4	3.9
Port Stanley	116	28	46	1.6	4.4	3.8	119	13	45	3.5	−0.2	3.6

Phase zero is December solstice. Phases marked * are unreliable owing to the small amplitude.

Table 4
Model-data comparisons for Night NmF2, 02 LT: amplitudes and phases for $F_{10.7} = 140$

Station	Time-GCM-CCM3						Ionosonde data					
	Amplitude (10^{10} m^{-3})				Phase (month)		Amplitude (10^{10} m^{-3})				Phase (month)	
	N_0	N_1	N_2	N_2/N_1	Φ_{N_1}	Φ_{N_2}	N_0	N_1	N_2	N_2/N_1	Φ_{N_1}	Φ_{N_2}
Moscow	3.8	2.5	1.7	0.7	4.9	3.3	19	12	2	0.2	6.0	0*
Slough	8.8	5.5	3.3	0.6	0.8	2.6	24	13	1	0.1	6.0	5*
Wakkanai	16.8	13.0	8.1	0.6	1.2	3.0	32	18	4	0.2	5.6	4*
Wallops Is	11.4	7.6	2.2	0.3	1.1	3*	29	6	3	0.5	5.4	3.6
Brisbane	9.9	3.9	3.3	0.8	5.1	3.5	43	21	3	0.1	0.3	4*
Hobart	6.8	1.9	1.9	1.0	4.1	4.0	20	11	2	0.2	0.2	4*
Port Stanley	5.0	4.0	3.3	0.8	5.0	4.5	38	35	7	0.2	−0.2	5*

Phase zero is December solstice. Phases marked * are unreliable owing to the small amplitude.

correctly represents the phase Φ_{N1} (peak near winter solstice). At the northern stations, TIME-GCM accurately gives the semiannual amplitude and phase (peak near equinoxes), and does well at Port Stanley except for the relatively small annual component, while Brisbane, the lowest latitude station in the set, has a notably large semiannual component. The ratios N_2/N_1 in Table 3 show that, progressing from north to south, there is a gradual shift from a predominantly annual variation to a predominantly semiannual variation, in both the model outputs and the ionosonde data, but with longitude differences as just mentioned. This corresponds to the behaviour mentioned in Section 3.2. At night (Table 4), the model badly underestimates NmF2 in summer, which leads to much too small values of N_0 and N_1, and the semiannual component is so small at all stations, both in model and data, that the values of N_2 are not reliable. Nevertheless, the equinoctial maxima do appear in almost all cases, which suggests they have some reality.

The most detailed study of the Fourier annual and semiannual components of NmF2 known to us is that of Yonezawa (1971), which was based on ionosonde data from about 20 stations at middle and low latitudes (he did not include Port Stanley). His results are difficult to compare directly with ours, because he split the 12-month component into 'seasonal' and 'non-seasonal' parts, but the general trends are consistent with our analysis of ionosonde data (Tables 3 and 4). Yonezawa found that the (semiannual/mean) amplitude ratio at noon decreases steadily from about 0.3 at latitude 25° to 0.15 at latitude 55°, but at midnight it is only about 0.15 at all latitudes; and that the semiannual phase is always very consistent, with maxima soon after equinox.

3.5. Comparison of Fourier components of NmF2 and [O/N_2] ratio

In Fig. 2 we see that the [O/N$_2$] ratio (R) varies throughout the year in a similar manner to NmF2. We test this resemblance in more detail by computing the annual and semiannual components of this ratio and comparing them with those of NmF2. In Table 5 (unlike Tables 3 and 4) the amplitudes are normalized to the annual mean values R_0 and N_0, and we show the ratio R_0/N_0 instead of the actual values of N_0 (which appear in Table 3). The values

Table 5
Annual and semiannual components for the $[O/N_2]$ ratio R at the F2 peak, and of the peak electron density NmF2, expressed as relative amplitudes and phases measured from December solstice

Station	Geog. lat. deg	Time-GCM-CCM3 $[O/N_2]$ ratio					TIME-GCM-CCM3 electron density				
		Amplitude			Phase (month)		Amplitude (10^{10} m^{-3})			Phase (month)	
		R_0	R_1/R_0	R_2/R_0	Φ_{R_1}	Φ_{R_2}	N_0/R_0	N_1/N_0	N_2/N_0	Φ_{N_1}	Φ_{N_2}
Moscow	56N	6.88	0.83	0.07	0.5	3*	25.5	0.79	0.07	1.0	3*
Slough	52N	5.98	0.70	0.08	0.5	3.4	26.9	0.71	0.20	0.9	3*
Wakkanai	45N	4.77	0.41	0.24	1.2	3.5	30.6	0.51	0.12	1.3	3.5
Wallops Is	39N	4.87	0.48	0.15	0.7	3.6	27.7	0.53	0.12	0.9	4*
Brisbane	28S	4.60	0.17	0.18	0.9	3.4	26.9	0.19	0.32	1.1	3.3
Hobart	43S	4.92	0.36	0.18	5.8	3.5	24.4	0.33	0.24	5.2	3.7
Port Stanley	52S	4.39	0.22	0.34	5.8	3.8	26.4	0.24	0.40	4.4	3.8

Also shown is the annual mean R_0 and the ratio N_0/R_0 of the annual means of NmF2 and $[O/N_2]$. Phases marked * are unreliable owing to the small amplitude. All values are for noon from the TIME-GCM model for $F_{10.7} = 140$.

of this ratio are fairly constant between the seven stations, implying that the electron density is largely controlled by the neutral chemistry. At each station the amplitude ratios N_1/N_0 and N_2/N_0 are fairly similar to the corresponding ratios R_1/R_0 and R_2/R_0, showing that the correspondence between NmF2 and $[O/N_2]$ ratio holds for the variations as well as for the mean value. This reinforces the idea that both annual and semiannual variations of F2-layer electron density are largely driven by changes of neutral composition (Millward et al., 1996b), which in turn can only be a consequence of the global thermospheric circulation (Rishbeth et al., 2000a).

In Table 5, the annual phases of $[O/N_2]$ and NmF2 are the same within about 0.5 month, except for the 1.4 month difference in annual phase at Port Stanley; the semiannual phases also agree well, and consistently lag behind equinox (phase 3.0) by about 0.5 month. At northern stations the annual phase lags behind winter solstice by 0.5–1.3 months, roughly consistent with the time-constant of order 20 days for seasonal changes of thermospheric composition estimated by Rishbeth et al. (2000a). In the south the behaviour is more complicated; at Brisbane, $[O/N_2]$ and NmF2 peak about a month after summer solstice, but at Hobart and Port Stanley NmF2 peaks in late fall and the annual phase slightly precedes winter solstice.

3.6. Variations and Fourier components of the height hmF2

Tables 6 and 7 show Fourier components of noon and night hmF2. The ionosonde values, derived from F2-layer 'MUF 3000 km factors' using the formula of Bilitza et al. (1979), are taken from Rishbeth et al. (2000b) who did not analyse data from Hobart or Brisbane; but they did analyse data from Norfolk Island, 1500 km east of Brisbane for which it provides an acceptable substitute. At all stations the mean height is 40–50 km higher at night than by day, except at Port Stanley where the night/day difference is 93 km, attributable to the strength of the thermospheric winds in the South Atlantic region. The annual phase Φ_{h1}, is such that hmF2 is higher in summer than in winter (in the south, hmF2 is greatest in early summer), both by day and by night. By day the agreement between model and data is quite satisfactory for the mean and the annual component, but poor at night. The semiannual variation is barely significant, its phase being poorly determined in the presence of the much larger annual amplitude, so much so that the semiannual phases for TIME-GCM shown in Tables 6 and 7 are imprecise, like those of electron density. Nor do the temperature curves in Figs. 2 and 3 show much sign of semiannual variation.

It is noticeable that in the ionosonde data, and to some extent in the TIME-GCM results, the semiannual variations of hmF2 are strong where NmF2 has a predominately annual variation, and vice versa. So the semiannual variations of hmF2 and NmF2 are different phenomena. As remarked by Rishbeth et al. (2000b), the ionosonde data clearly show a semiannual variation of hmF2 which TIME-GCM remarkably fails to reproduce at noon (except at Port Stanley), though the model does better at night (much the same applies to CTIP, as used by Zou et al., 2000).

Table 7 clearly reveals the cause of the serious discrepancies between model and ionosonde NmF2 at night: the model heights hmF2 are 30–70 km too low, implying that the TIME-GCM winds do not drive the layer high enough at night, and so the electron loss coefficient at the height hmF2 is much greater than it should be. Recent studies by Martinis et al. (2001) and Thuillier et al. (2002), comparing ground-based and space-based wind observations with current models, deal with equatorial and low latitude sites not directly relevant to the present study; nevertheless they point to the need for further validation work for thermospheric wind models.

Table 6
Model-data comparisons for Midday *h*mF2: amplitudes and phases for $F_{10.7} = 140$

Station	Geog. lat. deg	Time-GCM-CCM3 (12 LT) Amplitude (km) h_0	h_1	h_2	Phase (month) Φ_{h_1}	Φ_{h_2}	Ionosonde data (10-14 LT) Amplitude (km) h_0	h_1	h_2	Phase (month) Φ_{h_1}	Φ_{h_2}
Moscow	56N	260	14	2	5.5	4*	268	14	11	5.3	3.8
Slough	52N	258	13	4	5.3	4*	258	10	9	4.8	3.4
Wakkanai	45N	263	19	5	4.9	5*	272	19	11	5.3	3.7
Wallops Is	39N	265	12	3	4.6	4*	268	9	8	4.4	3.6
Brisb/Norfolk	28S	278	35	1	0.3	—	282	29	7	1.6	3.5
Hobart	43S	267	21	0	0.2	—	—	—	—	—	—
Port Stanley	52S	259	30	8	0.1	4*	261	40	10	1.1	3*

Phase zero is December solstice. Phases marked * are unreliable owing to the small amplitude. Ionosonde results come from Rishbeth et al. (2000b), who did not analyse data for Hobart; ionosonde data from Norfolk island (29S, 168E) are substituted for Brisbane.

Table 7
Model-data comparisons for Night *h*mF2, 02 LT: amplitudes and phases for $F_{10.7} = 140$

Station	Geog. lat. deg	Time-GCM-CCM3 (02 LT) Amplitude (km) h_0	h_1	h_2	Phase (month) Φ_{h_1}	Φ_{h_2}	Ionosonde data (22-02 LT) Amplitude (km) h_0	h_1	h_2	Phase (month) Φ_{h_1}	Φ_{h_2}
Moscow	56N	304	29	13	6.2	0.0	374	8	10	4.0	3.5
Slough	52N	313	37	9	6.2	0*	378	7	7	3.8	3.4
Wakkanai	45N	300	39	5	5.8	0*	366	8	6	5.0	3.5
Wallops Is	39N	304	20	7	6.4	0*	348	10	8	5.0	3.7
Brisb/Norfolk	28S	304	26	16	−0.4	0.3	340	17	6	2.0	2.9
Hobart	43S	311	21	7	−0.2	1*	—	—	—	—	—
Port Stanley	52S	352	47	12	−0.1	1*	387	9	8	3.4	3.8

Phase zero is December solstice. Phases marked * are unreliable owing to the small amplitude. Ionosonde results come from Rishbeth et al. (2000b), who did not analyse data for Hobart data; ionosonde data from Norfolk island (29S, 168E) are substituted for Brisbane.

4. The compositional *P*-parameter

4.1. Derivation

In trying to explain the seasonal changes, and to distinguish between the effects of composition changes, temperature changes and winds, the $[O/N_2]$ ratio is of limited use because it is very height-dependent. We need a parameter, evaluated at the F2 peak, which removes this complication and is unchanged when the height *h*mF2 is changed by thermal expansion and contraction or by meridional winds. This is the *P*-parameter, defined by Rishbeth and Müller-Wodarg (1999) and in a slightly different form by Rishbeth et al. (1987).

To derive the formula for *P*, we assume that, above a certain base height h_O (around 120 km) in the lower thermosphere, photochemistry is unimportant and so the major gases are distributed according to their own pressure scale heights. This is expected to be the case, except where there is strong vertical 'upwelling' or 'downwelling' which is unlikely to occur outside the auroral oval. Below h_O, the distributions of O and O_2 are determined by photochemical reactions, and the relative proportions of O, O_2 and N_2 may be affected by small-scale convective motions and turbulence. The 'photochemical' and 'diffusive' regimes may not be sharply bounded, but that does not change the essential argument. As before, we neglect any contribution of O_2 to the electron loss process, but that too should not affect the argument.

Let ζ denote 'reduced height' measured in units of the pressure scale height of atomic hydrogen (unit molar mass) from the base height h_O. This scale height is given by $H_1 = RT/g$, and is about 1000 km, where R is the universal gas constant, T is temperature, and g is the gravitational acceleration (As H_1 varies with height, the relation between ζ and real height h involves an integration, but this detail is not needed here).

The pressure scale heights of atomic oxygen and molecular nitrogen are in the ratio 28/16. Using the subscript 'o' to denote values of parameters at height h_O, and recalling that

(pressure) $\propto$ (temperature $\times$ concentration), the O and N_2 concentrations above h_O vary with ζ as:

$$[O] = (T_O/T)[O]_O \exp(-16\zeta), \tag{2a}$$

$$[N_2] = (T_O/T)[N_2]_O \exp(-28\zeta). \tag{2b}$$

Taking natural logarithms,

$$\ln[O] = \ln(T_O/T) + \ln[O]_O - 16\zeta, \tag{3a}$$

$$\ln[N_2] = \ln(T_O/T) + \ln[N_2]_O - 28\zeta. \tag{3b}$$

Multiplying (3a) and (3b) by 28 and 16 respectively, subtracting and moving to the right-hand side the terms relating to the height h_O:

$$28\ln[O] - 16\ln[N_2] + (28-16)\ln T - 448\zeta + 448\zeta = 28\ln[O]_O - 16\ln[N_2]_O + (28-16)\ln T_O. \tag{4}$$

Further collecting the terms, we define P as follows:

$$P = 28\ln[O] - 16\ln[N_2] + 12\ln T \tag{5}$$

which is equivalent at all heights ζ to

$$P_O = 28\ln[O]_O - 16\ln[N_2]_O + 12\ln T_O. \tag{6}$$

Hence the parameter P is height-independent provided O and N_2 are distributed vertically with their own scale heights, and that the temperature is constant at the height h_O (120 km). However, the temperature at 120 km does vary, and this must be taken into consideration, as noted below (though the changes at the F2-peak and at 120 km tend to offset one another, provided they are in the same sense, which is normally the case).

Absolute values of P have no significance, only changes are important. A change of +1 unit in P implies a change of +3.6% in [O], or of 6.2% in $[N_2]$, or of 8.3% in T or T_O, or some combination of these. The changes of composition, that cause changes in the P-parameter involve an entire column from the base height h_O to the top of the thermosphere. Vertical drifts due to winds can change the height hmF2, thus changing the $[O/N_2]$ ratio at that height but *not* the P-parameter.

To see how changes in daytime NmF2 are related to changes in composition, we need a relationship between P and the $[O/N_2]$ ratio (which is closely related to electron density, see Fig. 2); this relationship, however, varies with $[O/N_2]$. At most stations (Fig. 2), noon values of $[O/N_2]$ range from 1.6–2.3 in summer to an equinox/winter maximum of 6–8, though the winter maximum is 10 at Slough (and 14 at Moscow, not shown). From arithmetical calculations, it is found that the increase of $[O/N_2]$ ratio per unit increase of P varies from 5.0% for $[O/N_2] = 2$ to 6.0% for $[O/N_2] = 14$. As a useful 'working rule', we assume that a change of +1 unit in P represents a 5% increase of $[O/N_2]$ ratio at the noon F2 peak and also in NmF2, though this is a slight underestimate for larger values of $[O/N_2]$ ratio.

As mentioned above, allowance must be made for changes of neutral temperature, not only at the F2-peak but also at the 120 km base level. Outputs for 120 km from the TIME-GCM $F = 140$ simulation for 120 km are no longer available, so we used the empirical MSIS (Hedin, 1987) to estimate how the temperature T_O at 120 km varies throughout the day and the year. We find that both the day/night and seasonal changes in T_O at typical sites are within $\pm 5\%$, causing changes in P of about ± 0.5 unit which have no appreciable effect on our analysis.

4.2. Examples of composition changes

Fig. 4 shows the P-parameter for six stations at 12:00 and 02:00 LT; in all cases P is greater in winter than in summer. This confirms that the summer/winter changes in NmF2 are accompanied by changes in thermospheric composition, which by a rough calculation are sufficient to account for the change in NmF2.

For example, at Slough at 12:00 LT, the winter/summer change of P is 373–340 = 33 units. The 21% decrease of temperature from midsummer to midwinter adds 3 units to the change of P attributable to composition change, which is thus 36 units. By the 'working rule' just quoted (that each unit represents a change in $[O/N_2]$ by 5% or 0.05 in $\ln[O/N_2]$), 36 units corresponds to a change of 1.8 in $\ln[O/N_2]$ or a factor of 6.0 in $[O/N_2]$. Allowing for the effect of the large solar zenith angle in winter, this agrees with the factor of 4.6 change in Slough noon NmF2.

In the case of the fall and spring maxima of NmF2 at Port Stanley and Hobart, which occur in late April (around day 120) and October (around day 280), the fall/spring ratios of $[O/N_2]$ are about 1.2 at Port Stanley and 1.45 at Hobart, whereas at both stations the fall/spring ratio of NmF2 is about 1.7 and the fall/spring difference in P is 7 units, corresponding to a difference in $[O/N_2]$ of about 40%. At this season, the poleward winds are decreased (rather more at Port Stanley than at Hobart), which decreases downward drift and thus tends to increase NmF2. We conclude that the fall/spring differences of NmF2 are due to complicated interactions of composition changes and poleward wind, which are not the same at the two stations.

At all six stations there is a consistent day/night difference of about 10 units in P, of which the day/night change of temperature (e.g., by a factor of 1.15 in summer and 1.23 in winter at Slough) accounts for only 2 units. By the arguments of Section 4.1, the rest (about 8 units) must be attributed to day/night changes at the base level h_O around 120 km, i.e., to changes in one or more of the terms in Eq. (6). Day/night changes of T_O at 120 km account for only < 1 unit, so we conclude that the day/night changes in P are mostly due to composition changes, of which further investigation is needed. The short-term (day-to-day) fluctuations in P are discussed in Section 6.

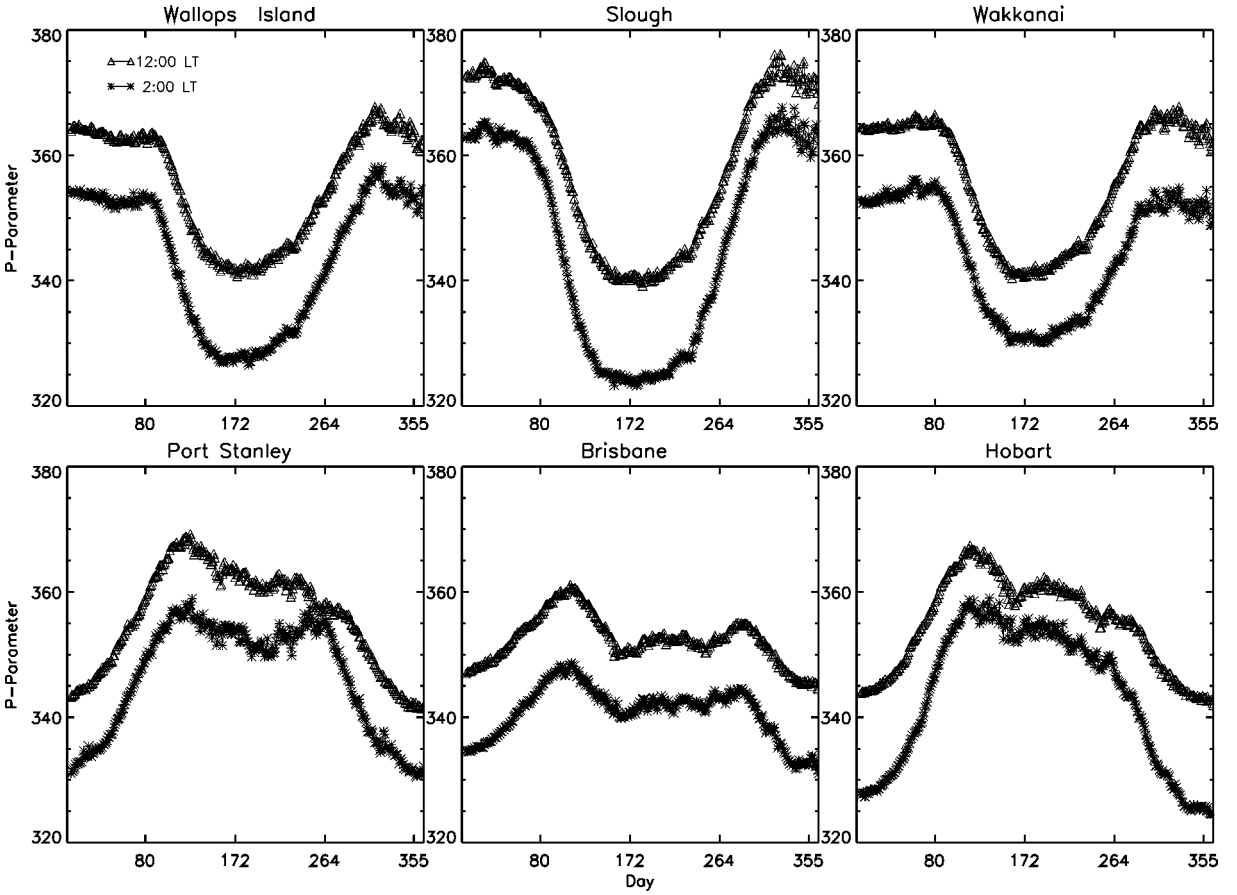

Fig. 4. *P*-parameter used to assess neutral composition changes (see text) for day (12:00 LT) and night (02:00 LT) calculated from TIME-GCM throughout the model year (see Section 4).

5. Day-to-day variability in the model and the data

In the previous sections we dealt with comparisons of model output and observations that were day versus night and seasonal. These are important validation time scales for assessing physical processes controlled, essentially, by the sun. We now address hourly characteristics of variability, as well as day-to-day patterns.

5.1. Local time effects of variability at two stations

Fig. 5 shows for each month the relative standard deviations $\sigma(N\mathrm{mF2})/N\mathrm{mF2}$ expressed as percentages, which we call the 'variability', for both the TIME-GCM-CCM3 model output and the ionosonde data at Slough (left) and Port Stanley (right). As before, the latter are averages over 6 years in which the solar activity is 'medium', corresponding to that in the model. As previously mentioned, the variability in the model outputs is due to two factors only: the 'meteorological' component mentioned in Section 1, due to disturbances propagated from the lower atmosphere, and the seasonal changes of solar illumination. The effect of the latter is most marked in equinox months, and is particularly seen near sunrise and sunset, but not so much near midday and midnight.

The two stations shown, Slough and Port Stanley, were selected to represent the range of midlatitude effects encountered in monthly mean behaviour. Both stations are 52° from the geographic equator and have similar variations of solar input in the course of a year. Their geomagnetic latitudes, however, differ by about 20° (Table 1), with Slough (50°N) a sub-auroral site ($L = 2.4$) and Port Stanley (30°S) only at $L = 1.3$. Thus the influence of auroral processes (such as joule heating) should be smaller at Port Stanley. Indeed, in our study of average variability at these sites, their patterns were decidedly sub-auroral versus midlatitude, as shown respectively in Figs. 6 and 7 of Rishbeth and Mendillo (2001). We do not show results for the other five stations, but comment on their similarities and differences where appropriate.

In examining the model-data comparisons in Fig. 5, two conclusions are suggested. First, in the model the variability

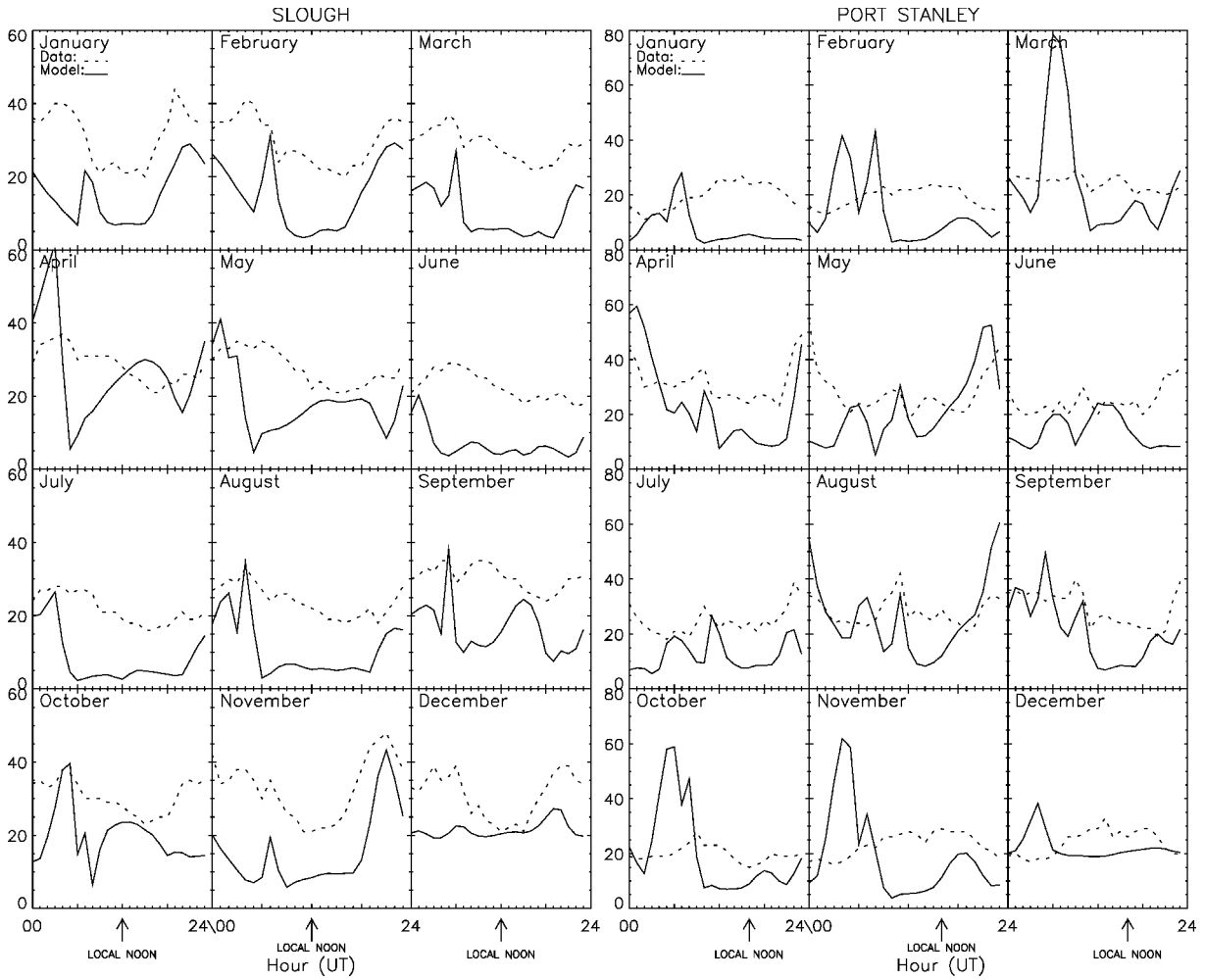

Fig. 5. Monthly plots of percentage variability $\sigma(N\mathrm{m}F2)/N\mathrm{m}F2$ versus UT for Slough and Port Stanley, from ionosonde data (dotted lines) and TIME-GCM-CCM3 (solid lines) as used in Fig. 1.

$\sigma(N\mathrm{m}F2)/N\mathrm{m}F2$ is generally of order 10% by day and 20–30% by night. The peaks around sunrise in months near equinox are largely due to the systematic shift in sunrise time throughout these months. As the pre-sunrise electron density is low, a change in sunrise time has a large percentage effect, and these peaks do not indicate true episodic variability. Similarly, the large daytime variability near the equinoxes at Slough (e.g., April, September and October) are simply due to the adjustment of the model's overestimate of wintertime behaviour, i.e., from the unrealistically large equinox transitions shown in Fig. 1. Excluding these cases, and considering there is no geomagnetic activity in the TIME- GCM simulation, we can only conclude that the CCM3 'meteorological' disturbances are the cause of much of the model variability. On a seasonal basis, their influence is least in summer (June–July at Slough and January–February at Port Stanley), when the model variability is $<10\%$, less than half of the total observed variability of $\sim$ 20%. In December, the daytime variability in the model at both stations is close to the observed variability, a feature seen also at the other five stations. The reasons for this December maximum of variability, due only to a 'meteorological' influence, are not known.

Even less expected are the large nighttime peaks of variability (60–80%) in the model results for Port Stanley in March, October and November (also $\sim$40% at Brisbane, not shown, though not at Hobart). At Slough, nighttime maxima occur in April ($\sim$60%) and in November ($\sim$40%), with somewhat similar patterns at Moscow, but not at Wallops Island. Again, since the model input does not contain the well-known equinoctial peak in geomagnetic activity (shown to affect variability at sub-auroral stations by Rishbeth and Mendillo, 2001), these nighttime features must be due to the CCM3 disturbances, with some contam-

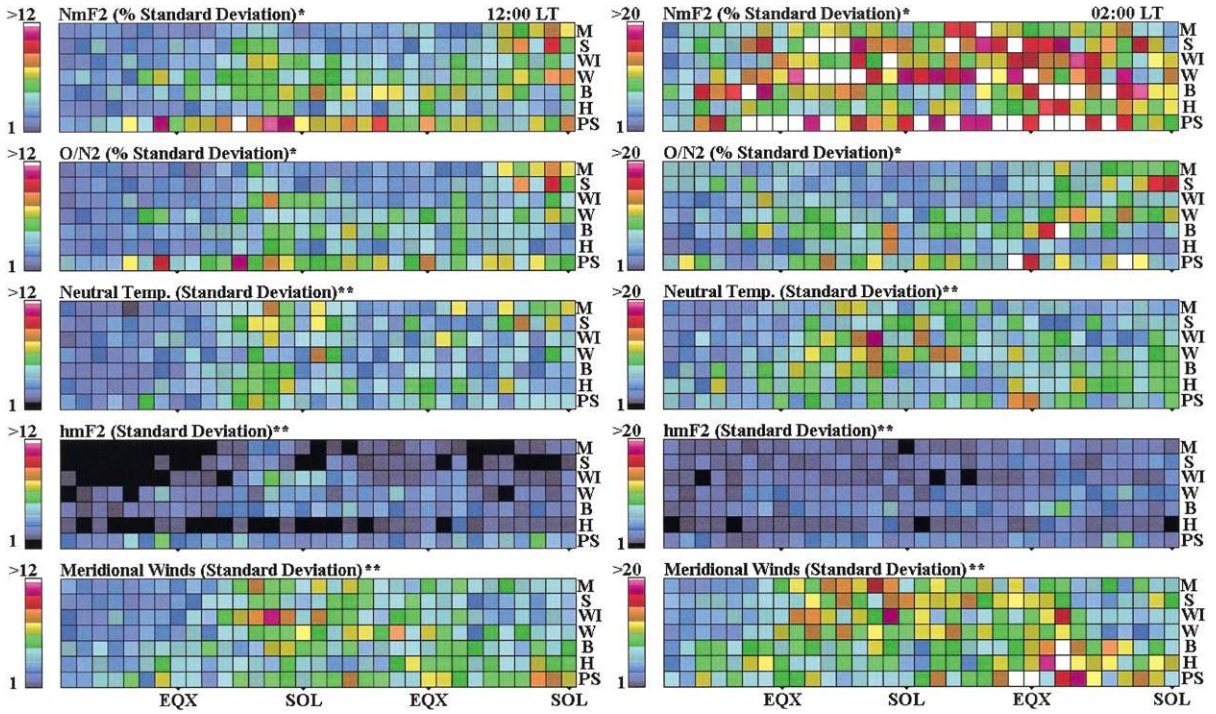

Fig. 6. 'Parameter quilts' showing standard deviations within 33 blocks of 11 days throughout the 'model year' at seven stations for each of five parameters (NmF2, etc.) at 12:00 LT and 02:00 LT. The colour scales show the percentage standard deviations of NmF2 and O/N_2 ratio (noted by *) and the absolute standard deviations of T_n(K), hmF2 (km) and meridional wind (m s^{-1}) (noted by **) within each 11-day block. The values within each block are de-trended to remove seasonal trends.

ination from the modelled equinox transition as described above.

5.2. Variability of parameters at individual stations for the model year

We now study the ionospheric disturbances that are produced by the imposed 'meteorological' disturbances. The original TIME-GCM-CCM3 runs were carried out some years ago and details of the meteorological inputs are no longer available. We therefore cannot study the origin of the disturbances, or how they are transmitted to the F2-layer from below, but we feel it worthwhile to study the general characteristics of the modelled day-to- day ionospheric variability.

For the present purpose, we divided the 70 sequences (five parameters, seven stations, 12:00 LT and 02:00 LT) into blocks and computed the standard deviations of the daily values within each block. We settled on 11-day blocks, and thus have 33 complete blocks spanning days 1–363 of the model year. We display the sequences of 33 standard deviations in colour-coded plots, which we call 'quilts' (Figs. 6 and 7). As marked on the plots, the March and September equinoxes fall in the 8th and 24th blocks and the June and December solstices in the 16th and 33rd blocks, respectively. The blue shading represents lowest variability, with red (and white) the greatest variability, as shown by the scales on the left. In the case of NmF2 and the $[O/N_2]$ ratio, we display the percentage standard deviation within each 11-day block; in the case of T_n(K), hmF2(km) and meridional wind (m s^{-1}), we plot the absolute standard deviations in those units. Before computing the standard deviations, the values within each block are de-trended to remove seasonal trends, which are usually greatest near the equinoxes.

In Fig. 6 the five 'quilts', one for each parameter, show the variability at the seven stations. We call these 'parameter quilts'. In Fig. 7 the seven 'quilts', one for each station, show the variability of the five parameters. We call these 'station quilts', and have kept the same numerical scale for each station on the 'parameter quilts', and similar scales for each parameter on the 'station quilts'.

In the noontime 'quilts', we see no overall coherent pattern, but some disturbed episodes stand out, particularly in northern stations in November and December (29th–33rd blocks) in NmF2, $[O/N_2]$ ratio and T_n; and also in May–June (13th–19th blocks approximately) at the lower latitude stations. Thus, as shown earlier in Fig. 5, winter is the most disturbed season in both hemispheres. Port Stanley's quilts show a high level of disturbance in NmF2 for much of the year, which might possibly be related to the strong

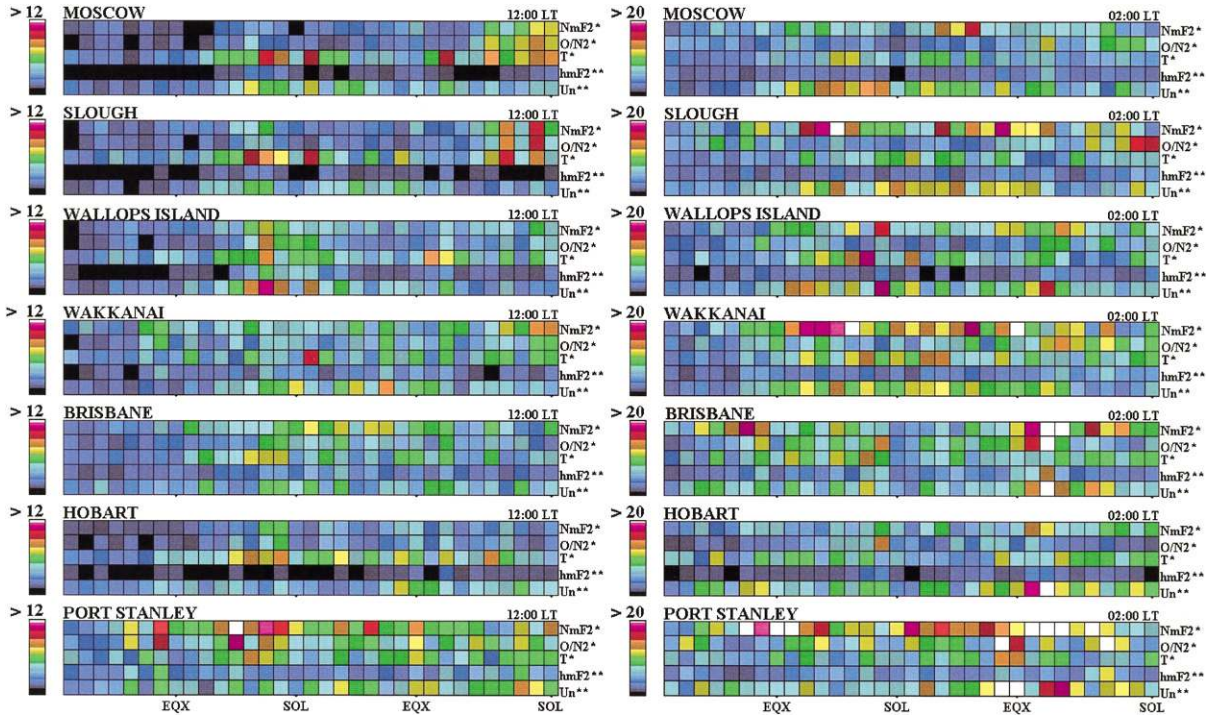

Fig. 7. 'Station quilts' showing standard deviations of five parameters (NmF2, etc.) within 33 blocks of 11 days throughout 'the model year' at each of seven stations at 12:00 LT and 02:00 LT. The colour scales show the percentage standard deviations of NmF2 and O/N_2 ratio (noted by *) and the absolute standard deviations of T_n(K), hmF2 (km) and meridional wind (m s^{-1}) (noted by **) within each 11-day block. The data within each block are de-trended to remove seasonal trends.

'meteorological' activity in the South Atlantic. There is little coherence between different parameters at one station, except between NmF2 and $[O/N_2]$, and weakly between some features of T_n, hmF_2 and meridional wind. At night there is even less coherence between parameters or between stations than by day, nor is there much detailed similarity between the night and day patterns in either the 'parameter quilts' or the 'station quilts'. We draw the following preliminary conclusions:

1. The disturbances occur more-or-less at random.
2. By day there is some correlation between NmF2 and $[O/N_2]$, as expected from F2-layer theory; and perhaps a weak correlation between hmF2 and meridional wind, again as expected.
3. The correlation between different places is very weak, suggesting that the scale size of the 'disturbances' is much less than global in scale, perhaps < 2500 km which is the smallest separation between any pair of our stations.
4. At night there is even less systematic behaviour than by day.
5. The de-trending has removed the equinox peaks in the variability of NmF2 that arose from the rapid changes in solar illumination and thermospheric composition at these times of year.

Conclusion 3 is consistent with the results of Rush (1976) who, using data from the world-wide ionosonde network, found a typical 'correlation distance' for the critical frequency foF2 of order 500 km north–south and 1000 km east–west. Further questions, such as the physics involved in the transmission of lower atmosphere disturbances to the ionosphere, and differences between northern and southern hemispheres, are reserved to future studies.

6. Case studies of disturbed periods

In Figs. 8 and 9 we show the variations of five model parameters at the F2 peak during two episodes of disturbance. We choose Port Stanley because the large-scale behaviour is quite well modelled by TIME-GCM, and because the 'quilts' suggest that 'meteorological' disturbances are strong at this site. As detailed information on the lower atmosphere inputs is not available, we confine discussion to the relations between parameters in two episodes of 25 and 20 days, chosen for their contrasting examples of how the disturbances affect the F2-layer.

In Episode 1 (days 265–290, Fig. 8), the peak electron density NmF2 shows quite large fluctuations and so do the height hmF2 and the meridional wind. In particular, the peak

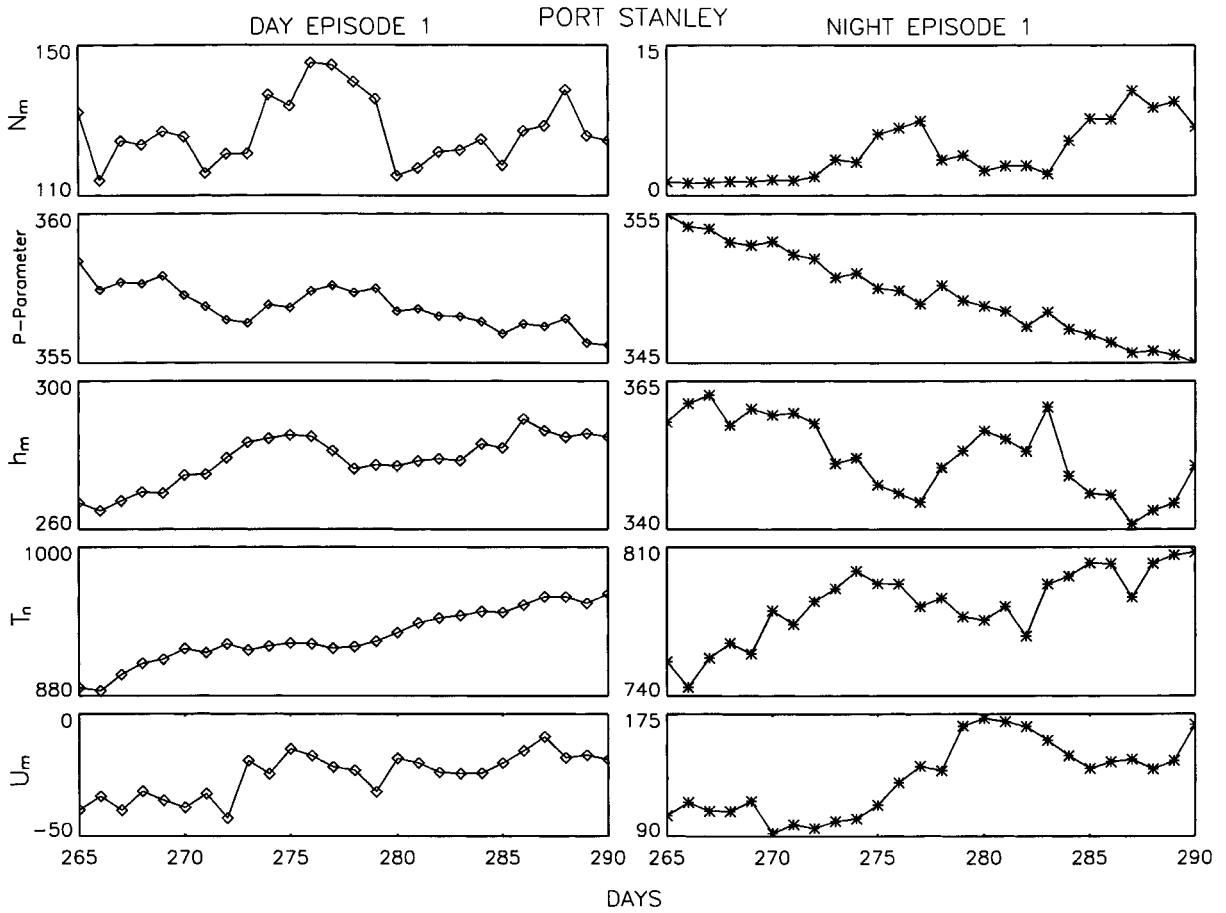

Fig. 8. Day-by-day and night-by-night model parameters at Port Stanley for 'Episode 1', days 265–290 at 12:00 LT (left) and 02:00 LT (right). Within each panel, top to bottom: Peak electron density NmF2 (10^{10} m^{-3}), P-parameter, height of peak (km), neutral temperature (K) and meridional wind (ms^{-1} positive northward).

of NmF2 at days 276–277 is about 20% greater than the mean of days 273 and 281, either side of this peak. However, the corresponding difference in P is only 1.0 unit which, by the 'working rule' of Section 4.1, accounts for only a 5% difference in NmF2. In Episode 2 (days 320–340, Fig. 9) NmF2 shows only small fluctuations (about $\pm$ 5%) by day superimposed on the background trend, though more at night. The day-to-day fluctuations of P are only $\pm$0.5 unit or smaller. We conclude that these fluctuations of NmF2 cannot be attributed to composition change, so we must look to other factors, namely wind and temperature.

By day (left-hand panels) the electron density fluctuations in Episode 1 show some correspondence with the fluctuations in height and wind, and thus appear to be driven by surges of equatorward wind superimposed on the ambient poleward flow. However, in Episode 2 the electron density fluctuations are smaller despite the large fluctuations in height that again follow abatements in the poleward wind. Neither episode shows significant correlation with temperature, and we conclude that both temperature and composition are stable by day, and little affected by wind-driven fluctuations.

At night (right-hand panels), the temperature fluctuations are more marked than by day, especially in Episode 1; rather surprisingly, they are almost uncorrelated with the height hmF2. Episode 1 shows considerable increases in NmF2, while Episode 2 shows a single period of decrease (days 325–326), correlated with a surge in the P-parameter and hmF2 but no correlation with temperature or winds. We do not think it worth trying to pursue the correlations in further detail here, though the general conclusion is that the day-to-day fluctuations are largely produced by fluctuations in the meridional wind, which move the layer bodily. The lack of significant change in P (daytime) is consistent with a time constant of days for changes at the lower boundary level h_O (Section 4.1). It seems that the day episodes and night episodes, though showing some resemblance, are not closely correlated.

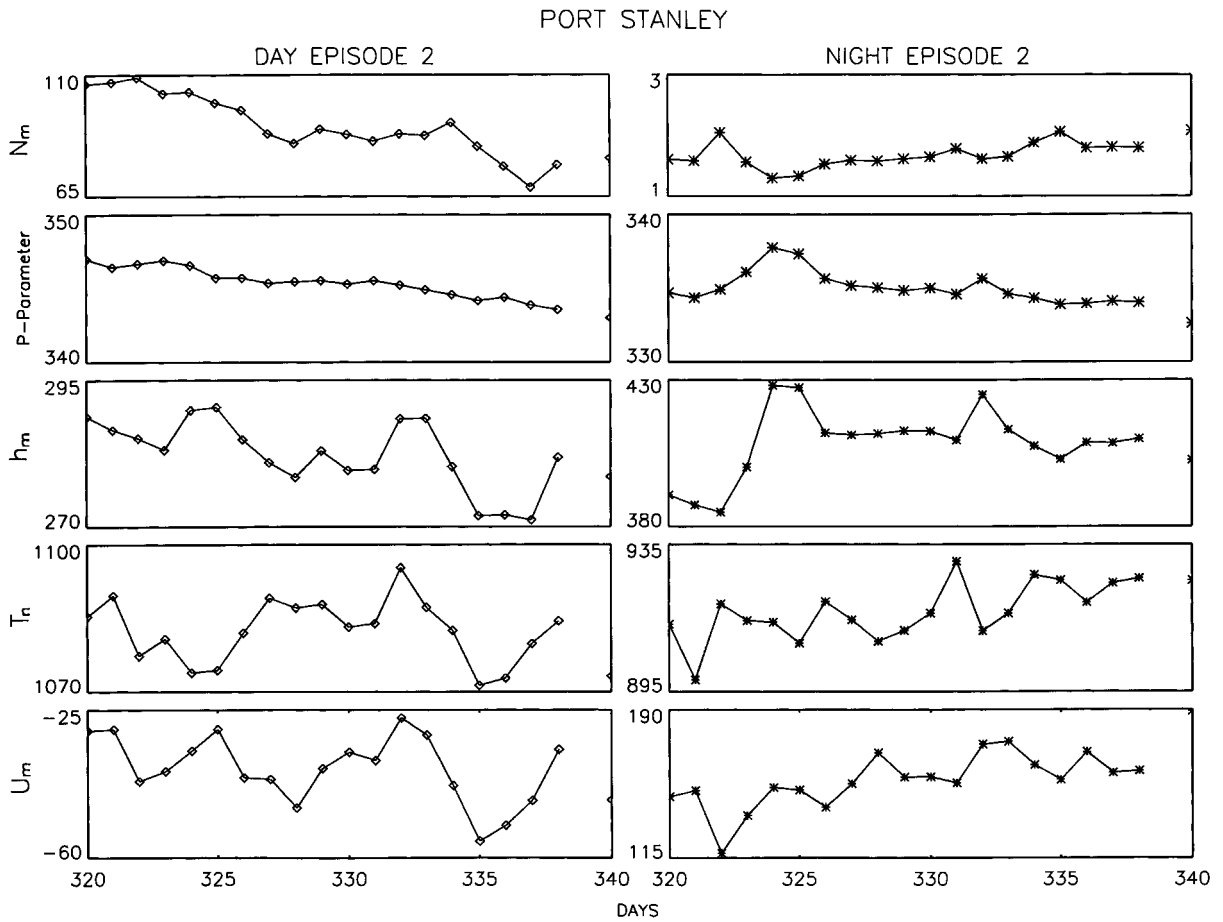

Fig. 9. Day-by-day and night-by-night model parameters at Port Stanley for 'Episode 2', days 320–340 at 12:00 LT (left) and 02:00 LT (right). Within each panel, top to bottom: Peak electron density NmF2 (10^{10} m^{-3}), P-parameter, height of peak (km), neutral temperature (K) and meridional wind (m s^{-1} positive northward).

A different situation (Episode 3, Fig. 10) occurs in early winter at Moscow and Slough, days 300–365. This prolonged period of activity can be seen in Fig. 2, and also in the 'quilts'. It is of interest because, as shown in Figs. 2 and 3, the [O/N$_2$] ratio is particularly high at this time of year. Around day 320, NmF2 fluctuates day-to-day by as much as 25%, while the day-to-day fluctuations of the P-parameter are about 3 units which corresponds to about 15% in electron density. Thus composition changes play a part in this winter episode, probably more than in the Port Stanley spring episodes 1 and 2, but nevertheless part of the variability of NmF2 must be attributed to fluctuations in winds and drifts. It is interesting that the fluctuations are quite well correlated at these two stations about 2500 km apart.

We should remember that the P-parameter depends on temperature, but that complication is very minor. At the F2-peak, the temperature fluctuations in the 'meteorological disturbances' are no more than about ±2% which corresponds to <1 unit of P. At the 120 km base level, we may expect them to be even smaller, as are the day/night and seasonal variations of temperature at that level.

Finally, we note that a 6–7 day quasi-periodicity appears in virtually all of the model parameters during this case study interval. With no external drivers in the model having this time scale, such as the solar wind sector boundary crossings influence of F-layer variability (Mendillo and Schatten, 1983), these wavelike disturbances must appear from coupling to lower altitudes. The origin and characteristics of such waves are discussed in Meyer and Forbes (1997).

7. Conclusions

In Sections 1 and 2 we presented the goals of a 'surface to exosphere' model, which we might regard as the ultimate objective, and how we have approached them. In Section 3 we examined the large-scale variations of F2-layer parameters, especially the peak electron density NmF2 by day

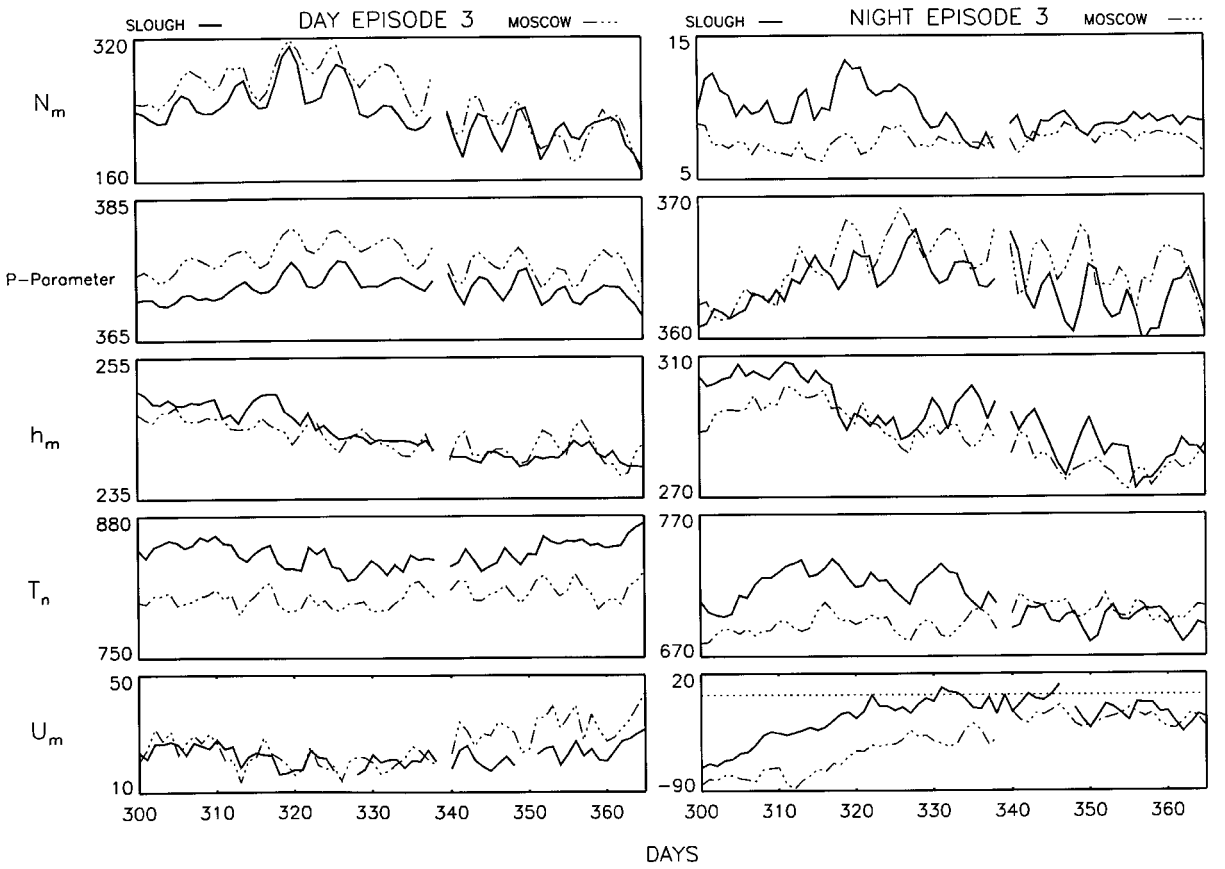

Fig. 10. Day-by-day and night-by-night model parameters at Slough (solid line) and Moscow (dashed line) for 'Episode 3', days 300–365 at 12:00 LT (left) and 02:00 LT (right). Within each panel, top to bottom: Peak electron density NmF2 (10^{10}m^{-3}), P-parameter, height of peak (km), neutral temperature (K) and meridional wind (m s^{-1} positive northward).

and night, at seven widely spaced ionosonde sites at mid-latitudes, for moderate solar activity (solar 10.7 flux =140 units) and geomagnetic calm. Our positive findings are that:

1. TIME-GCM models quite well the F2-layer behaviour at the seven sites.
2. In particular, the model captures the difference between the winter peaks seen in Europe and North America, and to a lesser extent in Australia, and the peaks near equinox seen in the South Atlantic and East Asia. These correspond respectively to the 'near-magnetic-pole' and 'far-from-magnetic-pole' sectors discussed by Rishbeth (1998) and Zou et al. (2000), and may be attributed to the characteristics of the global thermospheric circulation (Rishbeth et al., 2000a), an idea originated by Duncan (1969).
3. The seasonal and semiannual variations are closely associated with changes in thermospheric composition, in particular the $[O/N_2]$ ratio, which we studied in Section 4 with the aid of the height-independent P-parameter.
4. The peak height hmF2 is closely related to the neutral temperature, and is therefore strongly influenced by thermal expansion and contraction, and to a lesser extent by meridional winds.

In some respects the TIME-GCM simulations do not represent the ionosonde data so well:

1. They are 'over-tuned', in that summer-winter changes are overemphasized at most stations, in particular the northernmost stations, Moscow and Slough.
2. The peak height hmF2 is too low on summer nights, leading to very low values of NmF2.
3. The observed semiannual variations in hmF2 and in neutral temperature are not reproduced by TIME-GCM (or by CTIP, Rishbeth et al., 2000b);
4. Some other aspects require study, such as asymmetry between the equinoxes, notably the large 'fall maximum' of NmF2 at southern stations, which appear to be due more to winds rather than to composition changes.

In Sections 5 and 6, we studied the day-to-day fluctuations at the F2 peak. The greatest variability in the flux-coupled model occurs in the upper mesosphere and lower thermosphere. In the upper thermosphere (F2-layer), the variability arising in the lower atmosphere is damped by molecular diffusion, thermal conductivity and ion drag, and the solar EUV/UV and auroral forcings overwhelm the effects from the lower atmosphere. For the quiet geomagnetic conditions assumed here, we find that the disturbances propagating upward from the lower atmosphere cause variations in F2-layer electron density of order 10–30%, compatible with the conclusions reached by Forbes et al. (2000) and Rishbeth and Mendillo (2001). The 'quilts' presented in Section 5.2 show that the disturbances are almost uncorrelated between stations, though at any one station there is some correlation between different parameters, such as NmF2 and $[O/N_2]$ ratio. From the episodes discussed in Section 6, we conclude that fluctuations in winds are the main cause, but composition changes play some part in the day-to-day fluctuations of NmF2, at least in the winter episode 3.

The small day-by-day fluctuations in composition are consistent with the expected timescale of several days for large-scale changes of thermospheric composition. However, geomagnetic storms (not studied in this paper) provide an exception to this statement, because they produce drastic changes in hours by rapidly transporting air from auroral to middle latitudes: our analysis would not hold for that extreme type of forcing. We should also note that our analysis of F2-layer effects may not apply to violent meteorological storms with scale sizes smaller than the CCM3 grid.

We consider that this work has shown the feasibility of including day-to-day variability in the lower atmosphere in ionospheric modelling. We hope to follow it with further TIME-GCM-CCM3 runs that incorporate the variability of an actual year of meteorological, solar and geomagnetic activity.

Acknowledgements

We are grateful to Maura Hagan and Jeffrey Forbes for most valuable discussions, Ben Foster for extracting from archives the necessary TIME-GCM-CCM3 outputs, Ingo Müller-Wodarg and Cassandra Fesen for many helpful comments and suggestions, and World Data Centres A and C1 for Solar-Terrestrial Physics for their provision of data. This work was carried out under National Science Foundation Grant ATM 98 19848.

References

Akmaev, R.A., Forbes, J.M., Hagan, M.E., 1996. Simulation of tides with a spectral mesosphere/lower thermosphere model. Geophysical Research Letters 23, 2173–2176.

Anderson, D.N., Buonsanto, M.J., Codrescu, M., Decker, D., Fesen, C.G., Fuller-Rowell, T.J., Reinisch, B.W., Richards, P.G., Roble, R.G., Schunk, R.W., Sojka, J.J., 1998. Intercomparison of physical models and observations of the ionosphere. Journal of Geophysical Research 103, 2179–2192.

Andrews, D.G., Holton, J.R., Leovy, C.B., 1987. Middle Atmosphere Dynamics, International Geophysical Series, Vol. 40. Academic Press, New York, 487pp.

Bilitza, D., Sheikh, N.M., Eyfrig, R., 1979. A global model for the height of the F2-peak using M3000 values from the CCIR numerical map. Telecommunication Journal 46, 549–553.

Bilitza, D., Rawer, K., Bossy, L., Gulyaeva, T., 1993. International reference ionosphere—past, present and future. Advances in Space Research 13, 3.

Bougher, S.W., Engel, S., Roble, R.G., Foster, B., 1999. Comparative terrestrial planet thermospheres 2. Solar cycle variation of global structure and winds at equinox. Journal of Geophysical Research 104, 16,591–16,611.

Brasseur, G., Solomon, S., 1986. Aeronomy of the Middle Atmosphere, 2nd Edition. D. Reidel Publishing Co, Dordrecht, Holland.

Burkard, O., 1951. Die halbjährige Periode der F2-Schicht-Ionisation. Archiv Meteorologie und Bioklimatie. Wien 4, 391–402.

DeMore, W.B., et al., 1997. Chemical kinetics and photochemical data for use in stratospheric modeling, Evaluation Number 13. JPL Publication 97-4.

Dickinson, R.E., Ridley, E.C., Roble, R.G., 1981. A three-dimensional general circulation model of the thermosphere. Journal of Geophysical Research 86, 1499–1512.

Dickinson, R.E., Ridley, E.C., Roble, R.G., 1984. Thermospheric general circulation with coupled dynamics and composition. Journal of Atmospheric Science 41, 205–219.

Duncan, R.A., 1969. F-region seasonal and magnetic storm behaviour. Journal of Atmospheric and Terrestrial Physics 31, 59–70.

Fejer, B.G., Emmert, J.T., Shepherd, G.G., Solheim, B.H., 2000. Average daytime F-region disturbance neutral winds measured by UARS: initial results. Geophysical Research Letters 27, 1859–1862.

Fesen, C., Hysell, D., Meriwether, J.W., Mendillo, M., Fejer, B., Roble, R.G., Reinisch, B.W., Biondi, M.A., 2002. Modeling the low latitude atmosphere and ionosphere. Journal of Atmospheric and Solar-Terrestrial Physics 64, 1337–1349.

Fomichev, V.I., Blanchet, J.-P., Turner, D.S., 1998. Matrix parameterization of the 15 μm CO_2 band cooling in the middle and upper atmosphere for variable CO_2 concentration. Journal of Geophysical Research 103, 11,505–11,528.

Forbes, J.M., Palo, S.E., Zhang, X., 2000. Variability of the ionosphere. Journal of Atmospheric and Solar-Terrestrial Physics 62, 685–693.

Fuller-Rowell, T.J., Codrescu, M., Wilkinson, P., 2000. Quantitative modelling of the ionospheric response to geomagnetic activity. Annales Geophysicae 18, 766–781.

Hagan, M.E., Roble, R.G., Hackney, J., 2001. Migrating theromospheric tides. Journal of Geophysical Research 106, 12,739–12,752.

Hedin, A.E., 1987. The MSIS-86 thermospheric model. Journal of Geophysical Research 92, 4649–4662.

Hedin, A.E., et al., 1991. Revised global model of thermospheric winds using satellite and ground-based observations. Journal of Geophysical Research 96, 7657–7688.

Kiehl, J.T., Hack, J.J., Bonan, G.B., Boville, B.A., Williamson, D.L., Rasch, P.J., 1998. The National Center for Atmospheric

research community climate model: CCM3. Journal of Climate 11, 1131–1149.

King, J.W., Smith, P.A., 1968. The seasonal anomaly in the behaviour of the F2-layer critical frequency. Journal of Atmospheric and Terrestrial Physics 30, 1707–1713.

Lindzen, R.S., 1981. Turbulence and stress due to gravity wave and tidal breakdown. Journal of Geophysical Research 86, 9707–9714.

Martinis, C., Meriwether, J., Niciejewshi, R., Biondi, M., Fesen, C., Mendillo, M., 2001. Zonal neutral winds at equatorial and low latitudes. Journal of Atmospheric and Solar-Terrestrial Physics 63, 1559–1569.

Mendillo, M., Schatten, K., 1983. Influence of solar sector boundaries on ionospheric variability. Journal of Geophysical Research 88, 9145–9153.

Meyer, C.K., Forbes, J.M., 1997. A 6.5-day westward propagating planetary wave: origin and characteristics. Journal of Geophysical Research 102, 26,173–26,178.

Millward, G.H., Moffett, R.J., Quegan, S., Fuller-Rowell, T.J., 1996a. A coupled thermosphere–ionosphere–plasmasphere model (CTIP). In: Schunk, R.W. (Ed.), STEP Handbook of Ionospheric Models. Utah State University, Logan, Utah, pp. 239–280.

Millward, G.H., Rishbeth, H., Fuller-Rowell, T.J., Aylward, A.D., Quegan, S., Moffett, R.J., 1996b. F2 layer annual and semiannual variations. Journal of Geophysical Research 101, 5149–5156.

Richards, P.G., Fennelly, J.A., Torr, D.G., 1994. EUVAC: a solar EUV flux model for aeronomical calculations. Journal of Geophysical Research 99, 8981–8992.

Richmond, A.D., Ridley, E.C., Roble, R.G., 1992. A thermosphere/ionosphere general circulation model with coupled electrodynamics. Geophysical Research Letters 19, 601–604.

Rishbeth, H., 1998. How the thermospheric circulation affects the ionospheric F2-layer. Journal of Atmospheric and Solar-Terrestrial Physics 60, 1385–1402.

Rishbeth, H., Edwards, R.E., 1989. The isobaric F2-layer. Journal of Atmospheric and Terrestrial Physics 51, 321–338.

Rishbeth, H., Mendillo, M., 2001. Patterns of ionospheric variability. Journal of Atmospheric and Solar-Terrestrial Physics 63, 1661–1680.

Rishbeth, H., Müller-Wodarg, I.C.F., 1999. Vertical circulation and thermospheric composition: a modelling study. Annales Geophysicae 17, 794–805.

Rishbeth, H., Fuller-Rowell, T.J., Rees, D., 1987. Diffusive equilibrium and vertical motion in the thermosphere during a severe magnetic storm: a computational study. Planetary Space Science 35, 1157–1165.

Rishbeth, H., Zou, L., Müller-Wodarg, I.C.F., Fuller-Rowell, T.J., Millward, G.H., Moffett, R.J., Idenden, D.W., Aylward, A.D., 2000a. Annual and semiannual variations in the ionospheric F2-layer. II: physical discussion. Annales Geophysicae 18, 945–956.

Rishbeth, H., Sedgemore-Schulthess, K.J.F., Ulich, Th., 2000b. Semiannual and annual variations in the height of the ionospheric F2-peak. Annales Geophysicae 18, 285–299.

Roble, R.G., 1995. Energetics of the mesosphere and thermosphere. In: The Upper Mesosphere and Lower Thermosphere: a Review of Experiment and Theory, AGU Monograph, Vol. 87, pp. 1–21.

Roble, R.G., 1996. The NCAR thermosphere–ionosphere–mesosphere–electrodynamics general circulation model (TIME-GCM). In: Schunk, R.W., (Ed.), STEP Handbook on Ionospheric Models. Utah State University, pp. 281–288.

Roble, R.G., 2000. On the feasibility of developing a global atmospheric model extending from the ground to the exosphere. Geophysical Monograph, Vol. 123, American Geophysical Union, Washington DC, pp. 53–67.

Roble, R.G., Ridley, E.C., 1987. An auroral model for the NCAR thermosphere general circulation model (TGCM). Annales Geophysicae 5A, 369–382.

Roble, R.G., Ridley, E.C., 1994. A thermosphere–ionosphere–mesosphere–electrodynamics general circulation model (TIME-GCM): equinox solar cycle minimum simulations (30–500 km). Geophysical Research Letters 21, 417–420.

Roble, R.G., Dickinson, R.E., Ridley, E.C., 1987. On the global mean structure of the thermosphere. Journal of Geophysical Research 92, 8745–8758.

Roble, R.G., Ridley, E.C., Richmond, A.D., Dickinson, R.E., 1988. A coupled thermosphere/ionosphere general circulation model. Geophysical Research Letters 15, 1325–1328.

Rush, C.M., 1976. An ionospheric observation network for use in short-term propagation predictions. Telecommunications Journal 43 (VIII), 544.

Smith, A.K., 1996. Longitudinal variation in mesospheric winds: evidence for gravity wave filtering by planetary waves. Journal of Atmospheric Science 53, 1156–1173.

Thuillier, G., Wiens, R.H., Shepherd, G.G., Roble, R.G., 2002. Photochemistry and dynamics in thermospheric intertropical arcs measured by the WIND imaging interferometer on board UARS. Journal of Atmospheric and Solar-Terrestrial Physics 64, 405–415.

Wiens, R.H., Bhatnagar, V.P., Cogger, L.L., 1999. WINDII measurements of nightglow enhancements in the South Atlantic magnetic anomaly zone. Geophysical Research Letters 26, 2355–2358.

Yonezawa, T., 1971. The solar-activity and latitudinal characteristics of the seasonal, non-seasonal and semi-annual variations in the peak electron densities of the F2-layer at noon and at midnight in middle and low latitudes. Journal of Atmospheric and Terrestrial Physics 33, 889–907.

Zhao, X., Turco, R.P., 1997. Photodissociation parameterization for stratospheric photochemical modeling. Journal of Geophysical Research 102, 9447–9459.

Zou, L., Rishbeth, H., Müller-Wodarg, I.C.F., Aylward, A.D., Millward, G.H., Fuller-Rowell, T.J., Idenden, D.W., Moffett, R.J., 2000. Annual and semiannual variations in the ionospheric F2-layer. I: a modelling study. Annales Geophysicae 18, 927–944.